System-Level Security Solution for Hybrid D2D Communication in Heterogeneous D2D-Underlaid Cellular Network

Shaohan Feng, *Member, IEEE*, Xiao Lu, *Member, IEEE*, Dusit Niyato, *Fellow, IEEE*, Yuan Wu, *Senior Member, IEEE*, Xuemin Shen, *Fellow, IEEE*, and Wenbo Wang, *Senior Member, IEEE*

***Abstract*— To alleviate the spectrum scarcity problem, exploiting the vast available spectrum provided by the Millimeter-Wave (mmWave) frequency band and underlaying cellular network by Device-to-Device (D2D) communication are two promising solutions. In this paper, we focus on D2D-underlaid cellular network, where the D2D communication is performed on a hybrid manner (i.e., operating over either mmWave or microwave frequency band). To secure the hybrid D2D communication against vigilant adversary, we apply covert communication to hide its presence. In particular, the D2D transmitters perform power control and communication mode switch as well as leveraging the cellular signal to avoid the transmission detection by the adversaries. We model the conflict between the D2D transmitters and adversaries in the framework of a two-stage Stackelberg game. The D2D transmitters are the leaders to maximize their utility subject to the constraints on communication covertness at the upper stage. The adversaries are the followers to minimize their detection errors at the lower stage. We apply stochastic geometry to mathematically characterize the network spatial configuration and consider a large-scale D2D-underlaid network, enabling the study from system-level perspective. We analyze the game equilibrium and obtain it by adopting a bi-level algorithm. Numerical results are provided and insightful conclusions are drawn. Compared with the conventional D2D communication, hybrid D2D communication shows a significant advantage regarding throughput under the same security requirement while weak resistance to the more stringent security requirement.**

***Index Terms*— Wireless security, covert communication, device-to-device communication, hybrid communication, stochastic geometry.**

Manuscript received 3 October 2023; revised 11 April 2024; accepted 2 July 2024. Date of publication 15 July 2024; date of current version 11 October 2024. This work was supported in part by the National Natural Science Foundation of China (NSFC) under Grant 62302446 and in part by the Provincial Universities Basic Research Project (Science and Technology) under Grant QRK23011. The work of Dusit Niyato was supported in part by the National Research Foundation, Singapore; in part by the Infocomm Media Development Authority under its Future Communications Research and Development Programme, Defence Science Organisation (DSO) National Laboratories through the AI Singapore Programme (AISG) under Award AISG2-RP-2020-019 and Award FCP-ASTAR-TG-2022-003; and in part by Singapore Ministry of Education (MOE) Tier 1 under Grant RG87/22. The work of Wenbo Wang was supported in part by NSFC under Grant 62362046; in part by NSFC through Yunnan Major Scientific and Technological Projects under Grant 202202AG050002; in part by the National Key Research and Development Program of China under Grant 2023YFB3308401; and in part by ChingMu Tech. Ltd., Research Project "WiTracker" under Grant KKF0202301252. The associate editor coordinating the review of this article and approving it for publication was J. Liu. *(Corresponding author: Wenbo Wang.)*

Shaohan Feng is with the School of Information and Electronic Engineering (Sussex Artificial Intelligence Institute), Zhejiang Gongshang University, Hangzhou 314423, China (e-mail: feng_shaohan@mail.zjgsu.edu.cn).

Xiao Lu is with Ericsson Canada Inc., Kanata, ON K2K 2V6, Canada (e-mail: xiao.lu@ericsson.com).

Dusit Niyato is with the College of Computing and Data Science, Nanyang Technological University, Singapore 639798 (e-mail: DNIYATO@ntu.edu.sg).

Yuan Wu is with the State Key Laboratory of Internet of Things for Smart City and the Department of Computer and Information Science, University of Macau, Taipa, Macau (e-mail: yuanwu@um.edu.mo).

Xuemin Shen is with the Department of Electrical and Computer Engineering, University of Waterloo, Waterloo, ON N2L 3G1, Canada (e-mail: sshen@uwaterloo.ca).

Wenbo Wang is with the Faculty of Mechanical and Electrical Engineering, and Yunnan Key Laboratory of Intelligent Control and Application, Kunming University of Science and Technology, Kunming 650500, China (e-mail: wenbo_wang@kust.edu.cn).

Color versions of one or more figures in this article are available at https://doi.org/10.1109/TWC.2024.3423351.

Digital Object Identifier 10.1109/TWC.2024.3423351

I. Introduction

TO ALLEVIATE the congestion in wireless traffic incurred by the contradiction between the scarce spectral resource and exponentially growing wireless data especially caused by multimedia traffic, implementing Millimeter-Wave (mmWave) communication is becoming a trend. The mmWave communication operates at the frequency band with wavelength less than 10 mm (i.e., mmWave frequency band) and hence is able to exploit huge amount of available bandwidth, making it a promising solution for addressing the spectrum scarcity problem [1]. However, compared with the conventional microwave communication, the radio link over the mmWave frequency band suffers high path loss, severe blockage, and fast variation, which inhibit seamless connectivity (reliability) to network nodes. In this case, performing the communication on a hybrid manner (i.e., communicating over either microwave or mmWave frequency band so as to leverage each other's advantages to offset their own disadvantages [2]) is able to address the aforementioned challenges. For example, we can transmit over the mmWave frequency band in the Line-of-Sight (LoS) scenario and exchange control information over the microwave frequency band in the Non-LoS (NLoS) scenario to aid the beam alignment of the communication over the mmWave frequency band [1].

Another promising solution to alleviate the congestion in wireless traffic is Device-to-Device (D2D) communication [3].

The D2D communication enables direct communication among proximal users in the absence of network facility [4]. By such, the D2D communication can be deployed to underlay cellular network and reuse the cellular spectrum while causing tiny interference to the Cellular Users (CUs). This can reduce the traffic load at the Base Stations (BSs), enhance the coverage for cell-edge users and, more importantly, improve the spectral efficiency [5].

A. Hybrid D2D Communication

Motivated by the advantages of hybrid and D2D communications, in this work, we consider a hybrid D2D communication, which enables direct communication among proximal users over either mmWave frequency band to achieve high throughput or microwave frequency band in case of blockage. However, the security issue of the hybrid D2D communication is a major concern and challenging to be addressed due to the following reasons:

- Due to the limit on-device capacity including battery and computing power, it is impractical to deploy the energy-consuming methods such as encryption to secure the hybrid D2D communication. Moreover, the encryption incurs extra signaling and communication overheads (e.g., key management), which induces a high probability of exposure.
- Worsely, compared with the conventional microwave communication, the hybrid D2D communication requests high transmission power to ensure the link reliability over the mmWave frequency band. This, however, significantly increases the probability of exposure.
- Furthermore, merely preventing the confidential message from interception is insufficient from the privacy preserving perspective. For example, the exposure of communication behavior may reveals some secrets (e.g., the communication frequencies of the network nodes can reveal their importance).

B. Covert Communication

To secure the hybrid D2D communication, we resort to covert communication,[1] also referred to undetectable communication, which is one of remarkable physical layer security approaches [4]. Covert communication has the ability to conceal legitimate communication by leveraging the inherent characteristics of the wireless medium (e.g., interference, noise, and fading), while maintaining a certain rate at the intended user. The covert communication provisions the following advantages. The covert communication does not consume additional energy and hence is applicable in securing the network with limit resource. Moreover, the covert communication does not incur extra signaling or communication overhead, which induces a low probability of exposure. Furthermore, by enabling undetectable communication while maintaining certain rate at the intended user, not only the confidential message is immune to interception but also the communication behavior can be hidden and, more importantly, the communication reliability can be guaranteed.

[1]The operation mechanism of covert communication and the conventional covertness techniques can be found in [6].

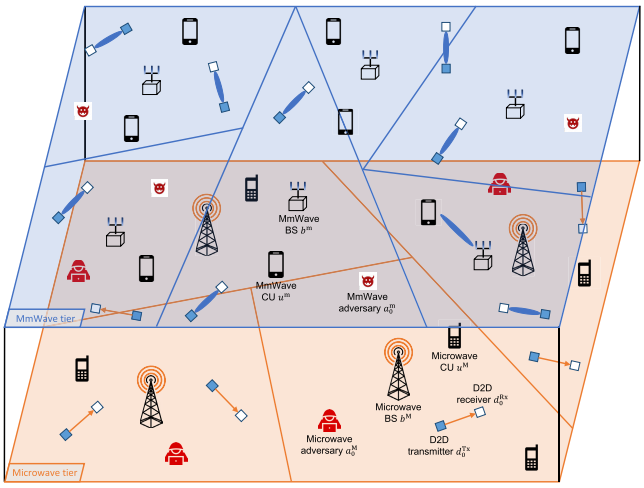

Fig. 1. Hybrid D2D communication underlaying heterogeneous downlink cellular networks threatened by adversaries.

C. Our Contributions

In this paper, we study a large-scale D2D-underlaid cellular network, containing massive BSs, CUs, D2D transmitters and receivers, and adversaries as shown in Fig. 1. Therein, the BSs communicate with CUs. The D2D transmitters and receivers perform hybrid D2D communication (i.e., communicating over either microwave or mmWave frequency band depending on the desired signal power received at D2D receivers). On the other hand, the adversaries aim to detect the D2D transmission. We secure the hybrid D2D communication against the adversaries with covert communication and by leveraging the cellular signal (i.e., signal transmitted by the cellular network). The cellular signal can cause interference dynamics in the received signal power at the adversaries and thereby distort their observation and further mislead their decision-making. By such, the cellular signal can be leveraged to hide the presence of D2D transmission. We model the conflict between the D2D transmitters and adversaries in the framework of a two-stage Stackelberg game, where the D2D transmitters are the leaders at the upper stage and the adversaries are the followers at the lower stage. At the lower stage, the adversaries aim at minimizing their detection errors so as to accurately detect the D2D transmission. At the upper stage, the D2D transmitters aim to maximize their utilities subject to the constraints on communication covertness. The key contributions of this paper are summarized as follows:

- We employ covert communication techniques to enhance the security of D2D communication in a D2D-underlaid cellular network. This approach addresses security challenges arising from limitations on device capacity.
- We apply the stochastic geometry and statistical channel model embedded mean-field approach to model the D2D-underlaid cellular network [7], where the network geographical configuration is characterized by using stochastic geometry. We derive the network performance metrics accordingly, aiming to conduct a system-level study.
- To model the competitive interaction between D2D users and adversaries, we formulate a two-stage Stackelberg

TABLE I
NOTATIONS AND THEIR TYPICAL VALUES

Symbol	Definition	Typical value
f, M (m)	Frequency band and microwave (mmWave) frequency band, respectively.	—
b^{f}, u^{f}, a^{f}, d^{Tx}, d^{Rx}	Indexes of microwave (mmWave) BS, microwave (mmWave) CU, microwave (mmWave) adversary if $\mathrm{f}=\mathrm{M}$ (m), D2D transmitter, and D2D receiver, respectively.	—
a_0^{f}, d_0^{Tx}, d_0^{Rx}	Indexes of typical microwave (mmWave) adversary if $\mathrm{f}=\mathrm{M}$ (m), typical D2D transmitter, and typical D2D receiver, respectively.	—
$\mathcal{B}^{\mathrm{f}}$, $\mathcal{U}^{\mathrm{f}}$, $\mathcal{A}^{\mathrm{f}}$, $\mathcal{D}^{\mathrm{Tx}}$	Sets of microwave (mmWave) BSs, microwave (mmWave) CUs, and microwave (mmWave) adversaries if $\mathrm{f}=\mathrm{M}$ (m), and that of D2D transmitters, respectively.	—
$\Phi_{\mathcal{B}^{\mathrm{f}}}$, $\Phi_{\mathcal{U}^{\mathrm{f}}}$, $\Phi_{\mathcal{A}^{\mathrm{f}}}$, $\Phi_{\mathcal{D}^{\mathrm{Tx}}}$	PPs of microwave (mmWave) BSs, microwave (mmWave) CUs, and microwave (mmWave) adversaries if $\mathrm{f}=\mathrm{M}$ (m), and that of D2D transmitters, respectively.	—
$\lambda_{\mathcal{B}^{\mathrm{f}}}$, $\lambda_{\mathcal{U}^{\mathrm{f}}}$, $\lambda_{\mathcal{A}^{\mathrm{f}}}$, $\lambda_{\mathcal{D}^{\mathrm{Tx}}}$	Densities of $\Phi_{\mathcal{B}^{\mathrm{f}}}$, $\Phi_{\mathcal{U}^{\mathrm{f}}}$, $\Phi_{\mathcal{A}^{\mathrm{f}}}$ for all $f\in\{\mathrm{M},\mathrm{m}\}$, and $\Phi_{\mathcal{D}^{\mathrm{Tx}}}$, respectively.	$5(10)\times10^{-2}/\mathrm{m}^2$, $5(10)\times10^{-1}/\mathrm{m}^2$, $1(2)\times10^{-2}/\mathrm{m}^2$, $10^{-1}/\mathrm{m}^2$ [4].
$\mathcal{C}_0^{\mathrm{f}}$, $\mathcal{C}_1^{\mathrm{f}}$, $\mathcal{M}^{\mathrm{f}}$, $\mathcal{D}_0$, $\mathcal{D}_1$	Events that microwave (mmWave) BS is mute and active and microwave (mmWave) communication mode if $\mathrm{f}=\mathrm{M}$ (m), and events that D2D transmitter is mute and active, respectively.	—
$\mathbb{P}^{\mathcal{C}_0^{\mathrm{f}}}$, $\mathbb{P}^{\mathcal{C}_1^{\mathrm{f}}}$, $\mathbb{P}^{\mathcal{M}^{\mathrm{f}}}$, $\mathbb{P}^{\mathcal{D}_0}$, $\mathbb{P}^{\mathcal{D}_1}$	Probabilities of events $\mathcal{C}_0^{\mathrm{f}}$, $\mathcal{C}_1^{\mathrm{f}}$, $\mathcal{M}^{\mathrm{f}}$ for all $f\in\{\mathrm{M},\mathrm{m}\}$, $\mathcal{D}_0$, and $\mathcal{D}_1$, respectively.	0.5, 0.5, —, 0.5, 0.5 [7].
p^{f}, τ^{f}, p^{D}, $p^{\mathcal{M}^{\mathrm{f}}}$	Cellular transmission power of microwave (mmWave) tier and power detection threshold of microwave (mmWave) adversaries if $\mathrm{f}=\mathrm{M}$ (m), D2D transmission power, and power threshold for switching communication mode, respectively.	30dBm, —, $[0,30]$ dBm, $[0,30]$ dBm.
α^{M}, $\alpha^{\mathrm{m,\,s}}$, ε, β, $u^{\mathrm{P,f}}$, u^{C}	Path-loss exponent over microwave frequency band, that over mmWave frequency band in $\mathrm{s}\in\mathcal{S}\triangleq\{\mathrm{LoS},\,\mathrm{NLoS}\}$ scenario, threshold of detection error, blockage parameter, reward of link reliability if $\mathrm{f}=\mathrm{M}$ (m), and power cost, respectively.	4, 2.5 (4) [8], 0.01, $\frac{1}{141.4}$ [9], 1 (100), 0.1.
$h^{\mathrm{f}}_{d_0^{\mathrm{Tx}}d_0^{\mathrm{Rx}}}$, $g^{\mathrm{m}}_{d_0^{\mathrm{Tx}}d_0^{\mathrm{Rx}}}$, υ^{s}	Small-scale fadings between typical D2D users over microwave (mmWave) frequency band if $\mathrm{f}=\mathrm{M}$ (m), antenna gain between typical D2D user over mmWave frequency band, and coefficient of small-scale fading over mmWave frequency band in LoS (NLoS) scenario, respectively.	$\exp(1)$ $\left(\mathrm{Gamma}\left(\upsilon^{\mathrm{s}},\frac{1}{\upsilon^{\mathrm{s}}}\right)\right)$, [10], $\upsilon^{\mathrm{s}}=4\,(1)$.
r_0, $\ell^{\mathrm{f}}(\cdot)$, η^{f}	D2D communication distance, and large-scale fading and SINR threshold at D2D receiver over microwave (mmWave) frequency band if $\mathrm{f}=\mathrm{M}$ (m), respectively.	1m, —, -10dB.
$N^{\mathrm{f}}_{d_0^{\mathrm{Rx}}}$, $N_{a_0^{\mathrm{f}}}$	Additive noise powers at D2D receiver d_0^{Rx} over microwave (mmWave) frequency band and microwave (mmWave) adversary if $\mathrm{f}=\mathrm{M}$ (m), respectively.	-90dBm [11].
f_e, F_e, $\mathcal{L}_e$, $\mathcal{L}_e^{-1}$	Probability Density Function (PDF), Cumulative Distribution Function (CDF), Laplace transform, and inverse Laplace transform of a random variable e, respectively.	—

game. In this framework, the adversaries act as followers, aiming to minimize their detection errors at the lower stage. The D2D users, on the other hand, act as leaders, aiming to maximize their utility while ensuring communication covertness at the upper stage.

- We analyze the equilibrium of the formulated Stackelberg game and obtain it by using a bi-level algorithm. We also verify the optimality of the obtained equilibrium. Additionally, we present numerical results to provide practical insights into the performance of the system.

D. Notation and Organization

The paper provides a summary of notations and their typical values in Table I. The subsequent sections are structured as follows: Section II offers a comprehensive review of the current state-of-the-art works. Section III details the system model, followed by the problem formulation and algorithm design in Section IV. The numerical results are presented in Section V, and Section VI concludes the paper by summarizing the findings.

II. Related Works

A. Hybrid D2D Communication

As discussed in Section I, there are two ways to meet the unprecedented demand of high-rate wireless communication (i.e., network desification such as D2D-underlaied cellular network [4] and deploying high frequency bands such as mmWave frequency band [2]). The D2D-underlaid cellular network enables the reuse of cellular spectrum for D2D communication, improving spectral efficiency and further overall network capacity, and, moreover, the direct communication between proximal user devices via D2D communication, reducing reliance on the traditional network infrastructure [4]. The mmWave frequency band offers a means to exploit the vast available bandwidth to achieve higher data rates [2].

The integration of D2D communication into cellular networks as an underlay has garnered significant attention for its potential to improve spectral efficiency from a spatial perspective. This approach allows for the reuse of cellular spectrum and has been extensively studied in the literature. For instance, the concept of a cognitive cellular network is explored in [12], where it serves as the primary network. Secondary users in this network have the option to transmit via either BS (BS mode) or D2D communication (D2D mode). An evolutionary game approach is employed to analyze the mode selection strategy of the secondary users, with performance metrics such as achieved data rate, power consumption, and bandwidth allocation being discussed. To enhance the communication reliability of cellular network, an energy mobile User Equipment Relay (UER) is introduced in [13] to relay information among CUs using D2D communication. As the UER needs to assist in data transmission for other CUs using its own power, an Energy Harvest (EH)-enabled UER is proposed,

ensuring that only harvested energy is consumed for relaying information. In another study [14], a D2D-underlaid cellular network is investigated, where D2D communication shares the spectrum of the uplink cellular network instead of the downlink, avoiding interference with the transmission of vital control information. A cooperative mode selection mechanism with power control and resource sharing is proposed in this context, aiming to maximize system capacity while maintaining the constraint on cellular Quality of Service (QoS).

The mmWave band, with its vast available bandwidth, holds promise as a carrier frequency for next-generation wireless networks and has found application in various commercial wireless systems [9]. These systems include IEEE 802.15.3c for personal area networking, IEEE 802.11ad for local area networking, and IEEE 802.16.1 for fixed-point access links. The coverage and data rate of mmWave cellular networks have been extensively studied in the literature [9]. One key aspect analyzed is the LoS probability, which is critical due to the nature of mmWave signals being sensitive to obstruction by physical objects. A distance-dependent LoS probability function is proposed to probabilistically depict the LoS and NLoS effects in mmWave communication scenarios. Comparative analysis between mmWave and Ultra High Frequency (UHF) cellular networks has demonstrated analytically the advantages of mmWave networks in terms of network coverage and data rate. In addition to cellular networks, mmWave technology has also been investigated for D2D communication networks [8]. Unlike previous works that assume all devices have exactly the same number of antennas, this study considers a practical scenario where the concurrent transmission beams may vary in width due to heterogeneous antenna arrays. The impact of such heterogeneous arrays on link performance is analyzed by deriving asymptotics, bounds, and approximations of SINR and rate distributions, providing insights into the performance of mmWave D2D networks.

B. Covert Communication

Secrecy becomes a more significant concern in mmWave communication compared with the conventional microwave communication due to the following factors inherent to the mmWave spectrum. First, the shorter wavelengths of mmWave signals make them more prone to being intercepted by adversaries using sophisticated equipment, especially in LoS scenarios where signals are less likely to be attenuated by obstacles. Second, the higher bandwidths available in mmWave bands enable higher data rates, making the transmitted information more valuable and hence more attractive to potential eavesdroppers. Third, the deployment of mmWave communication in emerging applications such as 5G and beyond introduces new security vulnerabilities and challenges that need to be addressed to ensure secure and reliable communication. In this case, various approaches have been proposed to enhance the secrecy of mmWave communication, including information-theoretical secrecy approach and encryption techniques [15], [16]. However, as discussed in Section I, merely preventing the interception of confidential messages is insufficient. To address this, covert communication, which enables the transmission of invisible communication signals, has emerged as a promising technique [17]. Covert communication offers several advantages. First, it provides a higher level of security compared to information-theoretical secrecy approach by concealing the communication signal from adversaries, thereby protecting the confidential message from interception. Second, unlike encryption, covert communication is independent of the information processing capability of the adversary. Third, covert communication can serve as an alternative or complementary solution to other security measures [18]. As a result, covert communication and its enhancement methods have been extensively studied. For example, the directional nature of mmWave communication has been leveraged in [19] to improve communication covertness. A beam training approach is designed to establish directional links, maximizing effective covert throughput. In another study [20], a full-duplex communication mode is considered to mask the presence of the legitimate transmitter. The jamming signal emitted by the transmitter varies over time to maintain a certain level of communication covertness over an extended period.

Motivated by the advantages of hybrid D2D communication, this paper investigates its application within a D2D-underlaid cellular network. In addition, recognizing the security threats inherent in hybrid D2D communication and the benefits of covert communication, we propose the use of covert communication techniques to enhance the security of the hybrid D2D communication.

III. System Model

We aim to secure D2D communication in a large-scale D2D-underlaid downlink cellular network against the adversaries from transmission detection[2] as shown in Fig. 1. The cellular network contains two tiers. The first tier operating at microwave frequency band, namely microwave tier, is denoted by M. The second tier operating at mmWave frequency band, namely mmWave tier, is denoted by m. The BSs of the microwave (mmWave) tier, namely microwave (mmWave) BSs, are equipped with omni-directional antennas (antenna arrays) and follow a Homogeneous Poisson Point Process (HPPP) $\Phi_{\mathcal{B}^{\mathrm{M}}}$ ($\Phi_{\mathcal{B}^{\mathrm{m}}}$) with density $\lambda_{\mathcal{B}^{\mathrm{M}}}$ ($\lambda_{\mathcal{B}^{\mathrm{m}}}$), where $\mathcal{B}^{\mathrm{M}}$ ($\mathcal{B}^{\mathrm{m}}$) is the set of microwave (mmWave) BSs [1]. Nearest-BS association policy is adopted for the cellular communication and the CUs at microwave (mmWave) tier, namely microwave (mmWave) CUs, follow an independent HPPP $\Phi_{\mathcal{U}^{\mathrm{M}}}$ ($\Phi_{\mathcal{U}^{\mathrm{m}}}$) with density $\lambda_{\mathcal{U}^{\mathrm{M}}} \gg \lambda_{\mathcal{B}^{\mathrm{M}}}$ ($\lambda_{\mathcal{U}^{\mathrm{m}}} \gg \lambda_{\mathcal{B}^{\mathrm{m}}}$) such that each microwave (mmWave) BS has at least one microwave (mmWave) CU in its Voronoi cell [21]. The microwave (mmWave) CUs are equipped with omni-directional antenna (antenna arrays). The D2D transmitters follow a HPPP $\Phi_{\mathcal{D}^{\mathrm{Tx}}}$ with density $\lambda_{\mathcal{D}^{\mathrm{Tx}}}$, where $\mathcal{D}^{\mathrm{Tx}}$ is the set of D2D transmitters. Each D2D transmitter serves a dedicated D2D receiver located

[2]One real-world application of the techniques investigated in this paper could be in military scenarios. Therein, the military units communicate directly with each other without relying on potentially insecure or compromised infrastructure to maintain the operation stealth. On the other hand, the adversaries attempt to detect the military transmission aiming to gather valuable information.

at r_0 in an arbitrary orientation. The D2D transmitters and their serving D2D receivers form D2D users (pairs). The D2D communication is performed on a hybrid manner. Namely, the D2D users work over either microwave or mmWave frequency band (i.e., operating at either microwave or mmWave communication mode denoted by $\mathcal{M}^{\mathrm{M}}$ and $\mathcal{M}^{\mathrm{m}}$, respectively). The D2D users are equipped with both the omni-directional antennas and antenna arrays for microwave and mmWave communication modes, respectively. ALOHA channel access scheme is adopted for both the cellular and D2D communications such that each microwave BS, each mmWave BS, and each D2D transmitter independently become active with the probabilities of $\mathbb{P}^{\mathcal{C}_1^{\mathrm{M}}}$, $\mathbb{P}^{\mathcal{C}_1^{\mathrm{m}}}$, and $\mathbb{P}^{\mathcal{D}_1}$, respectively[3] [21]. Correspondingly, each microwave BS, each mmWave BS, and each D2D transmitter independently remain mute with the probabilities of $\mathbb{P}^{\mathcal{C}_0^{\mathrm{M}}} \triangleq 1-\mathbb{P}^{\mathcal{C}_1^{\mathrm{M}}}$, $\mathbb{P}^{\mathcal{C}_0^{\mathrm{m}}} \triangleq 1-\mathbb{P}^{\mathcal{C}_1^{\mathrm{m}}}$, and $\mathbb{P}^{\mathcal{D}_0} \triangleq 1-\mathbb{P}^{\mathcal{D}_1}$, respectively. There exist adversaries at both the microwave and mmWave tiers, namely microwave and mmWave adversaries, respectively, aiming to detect the D2D transmission. Considering the randomness and unpredictability in the adversaries' behaviors, the spatial configuration of microwave (mmWave) adversaries follows an independent HPPP $\Phi_{\mathcal{A}^{\mathrm{M}}}$ ($\Phi_{\mathcal{A}^{\mathrm{m}}}$) with density $\lambda_{\mathcal{A}^{\mathrm{M}}}$ ($\lambda_{\mathcal{A}^{\mathrm{m}}}$) for the sake of practicality. The microwave (mmWave) adversaries are equipped with omni-directional antenna (antenna arrays). To analyze the network performance, we condition on that the D2D receiver geographically nearest to the origin is the typical D2D receiver and thereby denoted by D2D receiver d_0^{Rx} with spatial coordinate $\mathbf{x}_{d_0^{\mathrm{Rx}}}$. Accordingly, the D2D transmitter associated by D2D receiver d_0^{Rx} is the typical D2D transmitter and denoted by D2D transmitter d_0^{Tx} with spatial coordinate $\mathbf{x}_{d_0^{\mathrm{Tx}}}$. We consider that D2D transmitter d_0^{Tx} defends against the adversary that is geographically nearest (i.e., most threaten) to it. In this case, the microwave (mmWave) adversary that is geographically nearest to D2D transmitter d_0^{Tx} is regarded as the typical microwave (mmWave) adversary and denoted by microwave (mmWave) adversary a_0^{M} (a_0^{m}) with spatial coordinate $\mathbf{x}_{a_0^{\mathrm{M}}}$ ($\mathbf{x}_{a_0^{\mathrm{m}}}$). In return, microwave (mmWave) adversary a_0^{M} (a_0^{m}) aims to detect the transmission of D2D transmitter d_0^{Tx}.

A. Microwave Communication Model

The radio link over the microwave frequency band is subject to small-scale and large-scale fadings. We use the microwave communication between the typical D2D users (i.e., D2D transmitter d_0^{Tx} and D2D receiver d_0^{Rx}) as an example and the rest can be defined similarly. In particular, over the microwave frequency band, the received signal power at D2D receiver d_0^{Rx} regarding its associating D2D transmitter d_0^{Tx} is $y^{\mathrm{M}}_{d_0^{\mathrm{Tx}}d_0^{\mathrm{Rx}}} = p^{\mathrm{D}} h^{\mathrm{M}}_{d_0^{\mathrm{Tx}}d_0^{\mathrm{Rx}}} \ell^{\mathrm{M}}\left(\mathbf{x}_{d_0^{\mathrm{Tx}}}, \mathbf{x}_{d_0^{\mathrm{Rx}}}\right)$, where p^{D} is the D2D transmission power, and $h^{\mathrm{M}}_{d_0^{\mathrm{Tx}}d_0^{\mathrm{Rx}}}$ and $\ell^{\mathrm{M}}\left(\mathbf{x}_{d_0^{\mathrm{Tx}}}, \mathbf{x}_{d_0^{\mathrm{Rx}}}\right)$ measure the small-scale and large-scale fadings, respectively. Regarding the small-scale fading over the microwave frequency band, we adopt the Rayleigh fading channel model (i.e., independent and identical exponential distribution with unit mean $\exp(1)$) for tractability reason [18]. Another reason is that due to the long-range and ground-to-ground communication, NLoS dominates the communication status of the radio link over the microwave frequency band [22]. The large-scale fading for the microwave communication between the typical D2D users is $\ell^{\mathrm{M}}\left(\mathbf{x}_{d_0^{\mathrm{Tx}}}, \mathbf{x}_{d_0^{\mathrm{Rx}}}\right) \triangleq \left|\mathbf{x}_{d_0^{\mathrm{Tx}}} - \mathbf{x}_{d_0^{\mathrm{Rx}}}\right|^{-\alpha^{\mathrm{M}}} = r_0^{-\alpha^{\mathrm{M}}}$, where $\left|\mathbf{x}_{d_0^{\mathrm{Tx}}} - \mathbf{x}_{d_0^{\mathrm{Rx}}}\right|$ is the Euclidian distance in meter between the typical D2D users and $\alpha^{\mathrm{M}} \geq 2$ is the path-loss exponent over the microwave frequency band.

B. MmWave Communication Model

The radio link over the mmWave frequency band is subject to blockage effect, antenna gain, and large-scale and small-scale fadings [9]. Again, we use the mmWave communication between the typical D2D users as an example and the rest can be defined similarly. Specifically, over the mmWave frequency band, the received signal power of D2D receiver d_0^{Rx} regarding its associating D2D transmitter d_0^{Tx} is $y^{\mathrm{m}}_{d_0^{\mathrm{Tx}}d_0^{\mathrm{Rx}}} = p^{\mathrm{D}} h^{\mathrm{m}}_{d_0^{\mathrm{Tx}}d_0^{\mathrm{Rx}}} g^{\mathrm{m}}_{d_0^{\mathrm{Tx}}d_0^{\mathrm{Rx}}} \ell^{\mathrm{m}}\left(\mathbf{x}_{d_0^{\mathrm{Tx}}}, \mathbf{x}_{d_0^{\mathrm{Tx}}}\right)$, where $g^{\mathrm{m}}_{d_0^{\mathrm{Tx}}d_0^{\mathrm{Rx}}}$ is the antenna gain defined in Section III-B1, and $h^{\mathrm{m}}_{d_0^{\mathrm{Tx}}d_0^{\mathrm{Rx}}}$ and $\ell^{\mathrm{m}}\left(\mathbf{x}_{d_0^{\mathrm{Tx}}}, \mathbf{x}_{d_0^{\mathrm{Tx}}}\right)$ measures the small-scale and large-scale fadings, respectively, and are defined in Section III-B2.

1) Antenna Gain: Beamforming is adopted for directional mmWave communication. In particular, let $\theta_{\mathcal{D}^{\mathrm{Tx}}}$ and $\theta_{\mathcal{D}^{\mathrm{Rx}}}$ denote the beamwidth of D2D transmitters and D2D receivers, respectively, the main-lobe and side-lobe gains of the D2D transmitters' antenna arrays as well as those of the D2D receivers' antenna arrays are $G_{\mathcal{D}^{\mathrm{Tx}}}$, $g_{\mathcal{D}^{\mathrm{Tx}}}$, $G_{\mathcal{D}^{\mathrm{Rx}}}$, and $g_{\mathcal{D}^{\mathrm{Rx}}}$, respectively. The antenna gain between the typical D2D users is [10]

$$g^{\mathrm{m}}_{d_0^{\mathrm{Tx}}d_0^{\mathrm{Rx}}} = \begin{cases} G_{\mathcal{D}^{\mathrm{Tx}}}G_{\mathcal{D}^{\mathrm{Rx}}} & \text{w.p. } \frac{\theta_{\mathcal{D}^{\mathrm{Tx}}}}{2\pi}\frac{\theta_{\mathcal{D}^{\mathrm{Rx}}}}{2\pi}, \\ g_{\mathcal{D}^{\mathrm{Tx}}}G_{\mathcal{D}^{\mathrm{Rx}}} & \text{w.p. } \left(1-\frac{\theta_{\mathcal{D}^{\mathrm{Tx}}}}{2\pi}\right)\frac{\theta_{\mathcal{D}^{\mathrm{Rx}}}}{2\pi}, \\ G_{\mathcal{D}^{\mathrm{Tx}}}g_{\mathcal{D}^{\mathrm{Rx}}} & \text{w.p. } \frac{\theta_{\mathcal{D}^{\mathrm{Tx}}}}{2\pi}\left(1-\frac{\theta_{\mathcal{D}^{\mathrm{Rx}}}}{2\pi}\right), \\ g_{\mathcal{D}^{\mathrm{Tx}}}g_{\mathcal{D}^{\mathrm{Rx}}} & \text{w.p. } \left(1-\frac{\theta_{\mathcal{D}^{\mathrm{Tx}}}}{2\pi}\right)\left(1-\frac{\theta_{\mathcal{D}^{\mathrm{Rx}}}}{2\pi}\right), \end{cases} \tag{1}$$

where "w.p." is an abbreviation of "with probability". Let $g^{\mathrm{GG}}_{\mathcal{D}^{\mathrm{Tx}}\mathcal{D}^{\mathrm{Rx}}} = G_{\mathcal{D}^{\mathrm{Tx}}}G_{\mathcal{D}^{\mathrm{Rx}}}$, $g^{\mathrm{gG}}_{\mathcal{D}^{\mathrm{Tx}}\mathcal{D}^{\mathrm{Rx}}} = g_{\mathcal{D}^{\mathrm{Tx}}}G_{\mathcal{D}^{\mathrm{Rx}}}$, $g^{\mathrm{Gg}}_{\mathcal{D}^{\mathrm{Tx}}\mathcal{D}^{\mathrm{Rx}}} = G_{\mathcal{D}^{\mathrm{Tx}}}g_{\mathcal{D}^{\mathrm{Rx}}}$, $g^{\mathrm{gg}}_{\mathcal{D}^{\mathrm{Tx}}\mathcal{D}^{\mathrm{Rx}}} = g_{\mathcal{D}^{\mathrm{Tx}}}g_{\mathcal{D}^{\mathrm{Rx}}}$, $\mathbb{P}^{g^{\mathrm{GG}}_{\mathcal{D}^{\mathrm{Tx}}\mathcal{D}^{\mathrm{Rx}}}} = \frac{\theta_{\mathcal{D}^{\mathrm{Tx}}}}{2\pi}\frac{\theta_{\mathcal{D}^{\mathrm{Rx}}}}{2\pi}$, $\mathbb{P}^{g^{\mathrm{gG}}_{\mathcal{D}^{\mathrm{Tx}}\mathcal{D}^{\mathrm{Rx}}}} = \left(1-\frac{\theta_{\mathcal{D}^{\mathrm{Tx}}}}{2\pi}\right)\frac{\theta_{\mathcal{D}^{\mathrm{Rx}}}}{2\pi}$, $\mathbb{P}^{g^{\mathrm{Gg}}_{\mathcal{D}^{\mathrm{Tx}}\mathcal{D}^{\mathrm{Rx}}}} = \frac{\theta_{\mathcal{D}^{\mathrm{Tx}}}}{2\pi}\left(1-\frac{\theta_{\mathcal{D}^{\mathrm{Rx}}}}{2\pi}\right)$, and $\mathbb{P}^{g^{\mathrm{gg}}_{\mathcal{D}^{\mathrm{Tx}}\mathcal{D}^{\mathrm{Rx}}}} = \left(1-\frac{\theta_{\mathcal{D}^{\mathrm{Tx}}}}{2\pi}\right)\left(1-\frac{\theta_{\mathcal{D}^{\mathrm{Rx}}}}{2\pi}\right)$, the antenna gain between the typical D2D users can be simplified as $g^{\mathrm{m}}_{d_0^{\mathrm{Tx}}d_0^{\mathrm{Rx}}} = g^{\mathrm{g}}_{\mathcal{D}^{\mathrm{Tx}}\mathcal{D}^{\mathrm{Rx}}}$ w.p. $\mathbb{P}^{g^{\mathrm{g}}_{\mathcal{D}^{\mathrm{Tx}}\mathcal{D}^{\mathrm{Rx}}}}$ for all $\mathrm{g} \in \mathcal{G} \triangleq \{\mathrm{GG}, \mathrm{Gg}, \mathrm{gG}, \mathrm{gg}\}$. Similarly, the antenna gain between mmWave BSs and D2D receivers is denoted by $g^{\mathrm{g}}_{\mathcal{B}^{\mathrm{m}}\mathcal{D}^{\mathrm{Rx}}}$ w.p. $\mathbb{P}^{g^{\mathrm{g}}_{\mathcal{B}^{\mathrm{m}}\mathcal{D}^{\mathrm{Rx}}}}$ for all $\mathrm{g} \in \mathcal{G}$ and

[3]The microwave and mmWave BSs follow the ALOHA channel access scheme to be active over the considered frequency band.

that between D2D transmitters and mmWave adversaries is denoted by $g^{\mathrm{g}}_{\mathcal{D}^{\mathrm{Tx}}\mathcal{A}^{\mathrm{m}}}$ w.p. $\mathbb{P}^{g^{\mathrm{g}}_{\mathcal{D}^{\mathrm{Tx}}\mathcal{A}^{\mathrm{m}}}}$ for all $\mathrm{g} \in \mathcal{G}$.

2) Blockage Model: We adopt the blockage model in [9]. In particular, the probability that a radio link over the mmWave frequency band is LoS (NLoS) is $P^{\mathrm{LoS}}(r) = \exp(-\beta r)$ ($P^{\mathrm{NLoS}}(r) \triangleq 1 - P^{\mathrm{LoS}}(r)$), where r is the link length, β is a parameter determined by the density and size of the blockages with $\frac{1}{\beta}$ being called the average LoS range of the network. The blockage effect results in different large-scale fadings (i.e., the path-loss exponents over the mmWave frequency band in the LoS and NLoS scenarios are $\alpha^{\mathrm{m,\,LoS}}$ and $\alpha^{\mathrm{m,\,NLoS}}$, respectively). By such, the large-scale fading for the mmWave communication between the typical D2D users is that for all $\mathrm{s} \in \mathcal{S} \triangleq \{\mathrm{LoS}, \mathrm{NLoS}\}$,

$$\ell^{\mathrm{m,\,s}}\left(\mathbf{x}_{d_0^{\mathrm{Tx}}}, \mathbf{x}_{d_0^{\mathrm{Rx}}}\right) = \left|\mathbf{x}_{d_0^{\mathrm{Tx}}} - \mathbf{x}_{d_0^{\mathrm{Rx}}}\right|^{-\alpha^{\mathrm{m,\,s}}} = r_0^{-\alpha^{\mathrm{m,\,s}}} \text{ w.p. } P^{\mathrm{s}}(r_0). \tag{2}$$

Moreover, independent Nakagami fading is assumed with different fading parameters υ^{LoS} and $\upsilon^{\mathrm{NLoS}} \in \mathbb{Z}^+$ in LoS and NLoS scenarios, respectively [8]. By such, the small-scale fading between the typical D2D users over the mmWave frequency band (i.e., $h^{\mathrm{m}}_{d_0^{\mathrm{Tx}}d_0^{\mathrm{Rx}}}$) follows Gamma distribution with shape υ^{LoS} (υ^{NLoS}) and scale $\frac{1}{\upsilon^{\mathrm{LoS}}}$ ($\frac{1}{\upsilon^{\mathrm{NLoS}}}$) in the LoS (NLoS) scenario [8], which can be expressed as

$$h^{\mathrm{m,\,s}}_{d_0^{\mathrm{Tx}}d_0^{\mathrm{Rx}}} \sim \mathrm{Gamma}\left(\upsilon^{\mathrm{s}}, \frac{1}{\upsilon^{\mathrm{s}}}\right), \quad \forall \mathrm{s} \in \mathcal{S}. \tag{3}$$

C. Network Access Model

The D2D users can operate at either microwave or mmWave communication mode depending on the desired signal power at the D2D receivers [23]. For example, the typical D2D users will switch to mmWave communication mode (i.e., $\mathcal{M}^{\mathrm{m}}$) if the desired signal power at D2D receiver d_0^{Tx} over the mmWave frequency band is not lower than a predetermined threshold $p^{\mathcal{M}^{\mathrm{f}}}$ (i.e., $y^{\mathrm{m}}_{d_0^{\mathrm{Tx}}d_0^{\mathrm{Rx}}} \geq p^{\mathcal{M}^{\mathrm{f}}}$) and microwave communication mode (i.e., $\mathcal{M}^{\mathrm{M}}$) otherwise [24]. Hence, the probabilities that the typical D2D users are active at mmWave and microwave communication modes are

$$\mathbb{P}^{\mathcal{M}^{\mathrm{m}}} = \mathbb{P}\left[y^{\mathrm{m}}_{d_0^{\mathrm{Tx}}d_0^{\mathrm{Rx}}} \geq p^{\mathcal{M}^{\mathrm{f}}}\right] \tag{4}$$

and

$$\mathbb{P}^{\mathcal{M}^{\mathrm{M}}} = 1 - \mathbb{P}^{\mathcal{M}^{\mathrm{m}}}, \tag{5}$$

respectively, and the former is derived in Appendix A and numerically verified by checking the consistency between analytical and simulation results in Fig. 2(a). Note here that we use the Monte Carlo method and the parameter setting given in Table I to generate the simulation results. The parameter setting is the same in the rest of this paper.

1) D2D Communication at mmWave Communication Mode: The received signal power at D2D receiver d_0^{Rx} conditioned on the active status and mmWave communication mode of its associating D2D transmitter d_0^{Tx} (i.e., $\mathcal{D}_1 \cap \mathcal{M}^{\mathrm{m}}$) is $y^{\mathrm{m}}_{d_0^{\mathrm{Rx}}} = p^{\mathrm{D}} h^{\mathrm{m}}_{d_0^{\mathrm{Tx}}d_0^{\mathrm{Rx}}} g^{\mathrm{m}}_{d_0^{\mathrm{Tx}}d_0^{\mathrm{Rx}}} \ell^{\mathrm{m}}\left(\mathbf{x}_{d_0^{\mathrm{Tx}}}, \mathbf{x}_{d_0^{\mathrm{Rx}}}\right) + I^{\mathrm{C,\,m}}_{d_0^{\mathrm{Rx}}} + I^{\mathrm{D,\,m}}_{d_0^{\mathrm{Rx}}} + N^{\mathrm{m}}_{d_0^{\mathrm{Rx}}}$, where $I^{\mathrm{C,\,m}}_{d_0^{\mathrm{Rx}}} = p^{\mathrm{m}} \sum_{b^{\mathrm{m}} \in \left\{\mathcal{B}^{\mathrm{m}} | d_0^{\mathrm{Rx}}\right\}} \mathbb{1}_{b^{\mathrm{m}}} h^{\mathrm{m}}_{b^{\mathrm{m}}d_0^{\mathrm{Rx}}} g^{\mathrm{m}}_{b^{\mathrm{m}}d_0^{\mathrm{Rx}}} \ell^{\mathrm{m}}\left(\mathbf{x}_{b^{\mathrm{m}}}, \mathbf{x}_{d_0^{\mathrm{Rx}}}\right)$ is the interference from mmWave BSs, $I^{\mathrm{D,\,m}}_{d_0^{\mathrm{Rx}}} = p^{\mathrm{D}} \sum_{d^{\mathrm{Tx}} \in \left\{\mathcal{D}^{\mathrm{Tx}} \setminus \left\{d_0^{\mathrm{Tx}}\right\} | d_0^{\mathrm{Rx}}\right\}} \mathbb{1}_{d^{\mathrm{Tx}}} \mathbb{1}^{\mathcal{M}^{\mathrm{m}}}_{d^{\mathrm{Tx}}} h^{\mathrm{m}}_{d^{\mathrm{Tx}}d_0^{\mathrm{Rx}}} g^{\mathrm{m}}_{d^{\mathrm{Tx}}d_0^{\mathrm{Rx}}} \ell^{\mathrm{m}}\left(\mathbf{x}_{d^{\mathrm{Tx}}}, \mathbf{x}_{d_0^{\mathrm{Rx}}}\right)$ is that from other D2D transmitters that are active at mmWave communication mode, and $N^{\mathrm{m}}_{d_0^{\mathrm{Rx}}}$ is the additive noise at D2D receiver d_0^{Rx} over the mmWave frequency band. Therein, p^{m} is the transmission power of mmWave BSs, $\{\mathbf{x}_{b^{\mathrm{m}}}\}_{b^{\mathrm{m}} \in \left\{\mathcal{B}^{\mathrm{m}} | d_0^{\mathrm{Rx}}\right\}}$ is one of the realizations of the Point Process (PP) of mmWave BSs with D2D receiver d_0^{Rx} as the observation point (i.e., $\Phi_{\left\{\mathcal{B}^{\mathrm{m}} | d_0^{\mathrm{Rx}}\right\}}$) and $\{\mathbf{x}_{d^{\mathrm{Tx}}}\}_{d^{\mathrm{Tx}} \in \left\{\mathcal{D}^{\mathrm{Tx}} \setminus \left\{d_0^{\mathrm{Tx}}\right\} | d_0^{\mathrm{Rx}}\right\}}$ is that of D2D transmitters excluding D2D transmitter d_0^{Tx} with D2D receiver d_0^{Rx} as the observation point (i.e., $\Phi_{\left\{\mathcal{D}^{\mathrm{Tx}} \setminus \left\{d_0^{\mathrm{Tx}}\right\} | d_0^{\mathrm{Rx}}\right\}}$). $\mathbb{1}_{b^{\mathrm{m}}}$ is the active indicator of mmWave BS b^{m} and equal to 1 if mmWave BS b^{m} is active and 0 otherwise, and $\mathbb{1}_{d^{\mathrm{Tx}}}$ can be defined similarly. $\mathbb{1}^{\mathcal{M}^{\mathrm{m}}}_{d^{\mathrm{Tx}}}$ indicates the communication mode of D2D transmitter d^{Tx} and equals 1 (0) if D2D transmitter d^{Tx} is active at mmWave (microwave) communication mode. Consequently, conditioned on the active status and mmWave communication mode of D2D transmitter d_0^{Tx} (i.e., $\mathcal{D}_1 \cap \mathcal{M}^{\mathrm{m}}$), the SINR at D2D receiver d_0^{Rx} is $\mathrm{SINR}^{\mathrm{m}}_{d_0^{\mathrm{Rx}}} = \frac{p^{\mathrm{D}} h^{\mathrm{m}}_{d_0^{\mathrm{Tx}}d_0^{\mathrm{Rx}}} g^{\mathrm{m}}_{d_0^{\mathrm{Tx}}d_0^{\mathrm{Rx}}} \ell^{\mathrm{m}}\left(\mathbf{x}_{d_0^{\mathrm{Tx}}}, \mathbf{x}_{d_0^{\mathrm{Rx}}}\right)}{I^{\mathrm{C,\,m}}_{d_0^{\mathrm{Rx}}} + I^{\mathrm{D,\,m}}_{d_0^{\mathrm{Rx}}} + N^{\mathrm{m}}_{d_0^{\mathrm{Rx}}}}$. The reliability of the mmWave communication of the typical D2D users can be measured in terms of the successful transmission probability as follows:

$$\mathbb{P}\left[\mathrm{SINR}^{\mathrm{m}}_{d_0^{\mathrm{Rx}}} \geq \eta^{\mathrm{m}} \middle| \mathcal{D}_1 \cap \mathcal{M}^{\mathrm{m}}\right], \tag{6}$$

where η^{m} is the decoding threshold. The specific derivation of (6) is in Appendix B and numerically verified in Fig. 2(b). Note that there is a gap between the simulation and analytical results due to the approximation adopted in Appendix B. However, such a gap is tiny and hence negligible.

2) D2D Communication at Microwave Communication Mode: Similarly, the received signal power at D2D receiver d_0^{Rx} conditioned on the active status and microwave communication mode of its associating D2D transmitter d_0^{Tx} (i.e., $\mathcal{D}_1 \cap \mathcal{M}^{\mathrm{M}}$) is $y^{\mathrm{M}}_{d_0^{\mathrm{Rx}}} = p^{\mathrm{D}} h^{\mathrm{M}}_{d_0^{\mathrm{Tx}}d_0^{\mathrm{Rx}}} \ell^{\mathrm{M}}\left(\mathbf{x}_{d_0^{\mathrm{Tx}}}, \mathbf{x}_{d_0^{\mathrm{Rx}}}\right) + I^{\mathrm{C,\,M}}_{d_0^{\mathrm{Rx}}} + I^{\mathrm{D,\,M}}_{d_0^{\mathrm{Rx}}} + N^{\mathrm{M}}_{d_0^{\mathrm{Rx}}}$, where $I^{\mathrm{C,\,M}}_{d_0^{\mathrm{Rx}}} = p^{\mathrm{M}} \sum_{b^{\mathrm{M}} \in \left\{\mathcal{B}^{\mathrm{M}} | d_0^{\mathrm{Rx}}\right\}} \mathbb{1}_{b^{\mathrm{M}}} h^{\mathrm{M}}_{b^{\mathrm{M}}d_0^{\mathrm{Rx}}} \ell^{\mathrm{M}}\left(\mathbf{x}_{b^{\mathrm{M}}}, \mathbf{x}_{d_0^{\mathrm{Rx}}}\right)$ is the interference from microwave BSs, $I^{\mathrm{D,\,M}}_{d_0^{\mathrm{Rx}}} = p^{\mathrm{D}} \sum_{d^{\mathrm{Tx}} \in \left\{\mathcal{D}^{\mathrm{Tx}} \setminus \left\{d_0^{\mathrm{Tx}}\right\} | d_0^{\mathrm{Rx}}\right\}} \mathbb{1}_{d^{\mathrm{Tx}}} \left(1 - \mathbb{1}^{\mathcal{M}^{\mathrm{m}}}_{d^{\mathrm{Tx}}}\right) h^{\mathrm{M}}_{d^{\mathrm{Tx}}d_0^{\mathrm{Rx}}} \ell^{\mathrm{M}}\left(\mathbf{x}_{d^{\mathrm{Tx}}}, \mathbf{x}_{d_0^{\mathrm{Rx}}}\right)$ is that from other D2D transmitters that are active at microwave communication mode, and $N^{\mathrm{M}}_{d_0^{\mathrm{Rx}}}$ is the additive noise at D2D receiver d_0^{Rx} over the microwave frequency band. Therein, p^{M} is the transmission power of microwave BSs, $\{\mathbf{x}_{b^{\mathrm{M}}}\}_{b^{\mathrm{M}} \in \left\{\mathcal{B}^{\mathrm{M}} | d_0^{\mathrm{Rx}}\right\}}$ is one of the realizations of the PP of microwave BSs with D2D receiver d_0^{Rx} as the observation point (i.e., $\Phi_{\left\{\mathcal{B}^{\mathrm{M}} | d_0^{\mathrm{Rx}}\right\}}$) and $\{\mathbf{x}_{d^{\mathrm{Tx}}}\}_{d^{\mathrm{Tx}} \in \left\{\mathcal{D}^{\mathrm{Tx}} \setminus \left\{d_0^{\mathrm{Tx}}\right\} | d_0^{\mathrm{Rx}}\right\}}$ is that of D2D transmitters

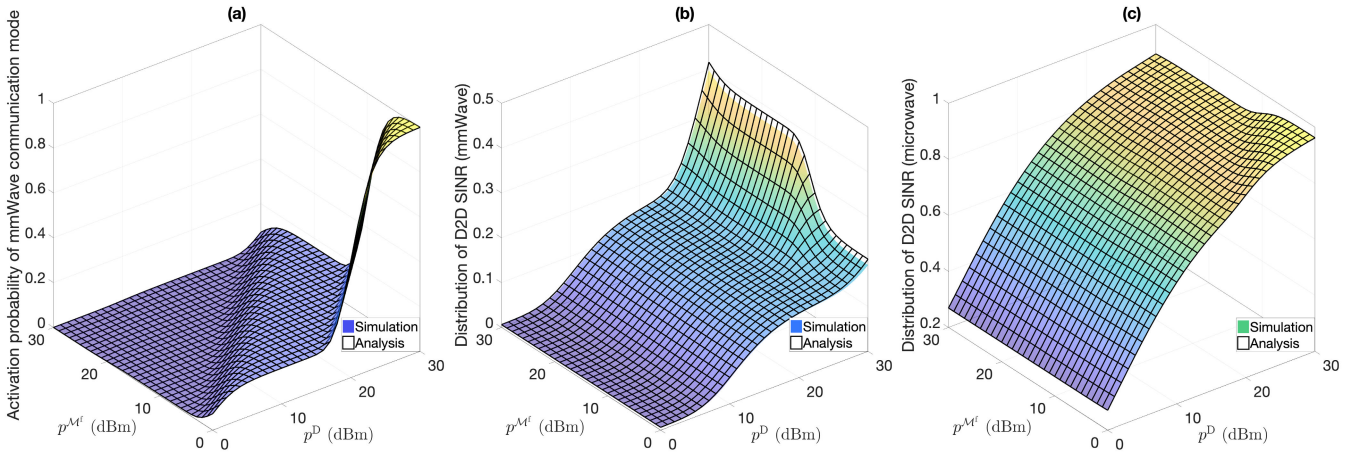

Fig. 2. Comparison between the simulation and analytical results on (a) the activation probability of mmWave communication mode, (b) the distribution of D2D SINR at mmWave communication mode, and (c) the distribution of D2D SINR at microwave communication mode.

excluding D2D transmitter d_0^{Tx} with D2D receiver d_0^{Rx} as the observation point (i.e., $\Phi_{\left\{\mathcal{D}^{\mathrm{Tx}}\setminus\left\{d_0^{\mathrm{Tx}}\right\}|d_0^{\mathrm{Rx}}\right\}}$). $\mathbb{1}_{b^{\mathrm{M}}}$ is the active indicator of microwave BS b^{M} and equal to 1 if microwave BS b^{M} is active and 0 otherwise. Consequently, conditioned on the active status and microwave communication mode of D2D transmitter d_0^{Tx} (i.e., $\mathcal{D}_1\cap\mathcal{M}^{\mathrm{M}}$), the SINR at D2D receiver d_0^{Rx} is $\mathrm{SINR}_{d_0^{\mathrm{Rx}}}^{\mathrm{M}}=\frac{p^{\mathrm{D}}h^{\mathrm{M}}_{d_0^{\mathrm{Tx}}d_0^{\mathrm{Rx}}}\ell^{\mathrm{M}}\left(\mathbf{x}_{d_0^{\mathrm{Tx}}},\mathbf{x}_{d_0^{\mathrm{Rx}}}\right)}{I^{\mathrm{C,\,M}}_{d_0^{\mathrm{Rx}}}+I^{\mathrm{D,\,M}}_{d_0^{\mathrm{Rx}}}+N^{\mathrm{M}}_{d_0^{\mathrm{Rx}}}}$. To guarantee that D2D receiver d_0^{Rx} can successfully decode the signal received over the microwave frequency band, its SINR has to be no less than a threshold η^{M} (i.e., $\mathrm{SINR}_{d_0^{\mathrm{Rx}}}^{\mathrm{M}}\geq\eta^{\mathrm{M}}$). This results in successful transmission probability for the microwave communication between the typical D2D users as follows:

$$\mathbb{P}\left[\mathrm{SINR}_{d_0^{\mathrm{Rx}}}^{\mathrm{M}}\geq\eta^{\mathrm{M}}\middle|\,\mathcal{D}_1\cap\mathcal{M}^{\mathrm{M}}\right],\tag{7}$$

and the derivation of which is in Appendix C and verified in Fig. 2(c).

D. Transmission Detection Model

As stated at the beginning of Section III, both microwave adversary a_0^{M} and mmWave adversary a_0^{m} aim to detect the transmission of D2D transmitter d_0^{Tx}. For mmWave adversary a_0^{m}, if D2D transmitter d_0^{Tx} is either mute or active at microwave communication mode (i.e., $\mathcal{D}_0\cup\left(\mathcal{D}_1\cap\mathcal{M}^{\mathrm{M}}\right)$), its received signal power is accordingly $y_{a_0^{\mathrm{m}}}=I^{\mathrm{C}}_{a_0^{\mathrm{m}}}+I^{\mathrm{D}}_{a_0^{\mathrm{m}}}+N_{a_0^{\mathrm{m}}}$. Therein, $I^{\mathrm{C}}_{a_0^{\mathrm{m}}}=p^{\mathrm{m}}\sum_{b^{\mathrm{m}}\in\left\{\mathcal{B}^{\mathrm{m}}|a_0^{\mathrm{m}}\right\}}\mathbb{1}_{b^{\mathrm{m}}}h^{\mathrm{m}}_{b^{\mathrm{m}}a_0^{\mathrm{m}}}g^{\mathrm{m}}_{b^{\mathrm{m}}a_0^{\mathrm{m}}}\ell^{\mathrm{m}}\left(\mathbf{x}_{b^{\mathrm{m}}},\mathbf{x}_{a_0^{\mathrm{m}}}\right)$ is the interference from mmWave BSs, $I^{\mathrm{D}}_{a_0^{\mathrm{m}}}=p^{\mathrm{D}}\sum_{d^{\mathrm{Tx}}\in\left\{\mathcal{D}^{\mathrm{Tx}}\setminus\left\{d_0^{\mathrm{Tx}}\right\}|a_0^{\mathrm{m}}\right\}}\mathbb{1}_{d^{\mathrm{Tx}}}\mathbb{1}^{\mathcal{M}^{\mathrm{m}}}_{d^{\mathrm{Tx}}}h^{\mathrm{m}}_{d^{\mathrm{Tx}}a_0^{\mathrm{m}}}g^{\mathrm{m}}_{d^{\mathrm{Tx}}a_0^{\mathrm{m}}}\ell^{\mathrm{m}}\left(\mathbf{x}_{d^{\mathrm{Tx}}},\mathbf{x}_{a_0^{\mathrm{m}}}\right)$ is that from D2D transmitters that are active at mmWave communication mode, and $N_{a_0^{\mathrm{m}}}$ is the additive noise at mmWave adversary a_0^{m}. Here, $\left\{\mathbf{x}_{b^{\mathrm{m}}}\right\}_{b^{\mathrm{m}}\in\left\{\mathcal{B}^{\mathrm{m}}|a_0^{\mathrm{m}}\right\}}$ is one of the realizations of the PP of mmWave BSs with mmWave adversary a_0^{m} as the observation point (i.e., $\Phi_{\left\{\mathcal{B}^{\mathrm{m}}|a_0^{\mathrm{m}}\right\}}$) and $\left\{\mathbf{x}_{d^{\mathrm{Tx}}}\right\}_{d^{\mathrm{Tx}}\in\left\{\mathcal{D}^{\mathrm{Tx}}\setminus\left\{d_0^{\mathrm{Tx}}\right\}|a_0^{\mathrm{m}}\right\}}$ is that of D2D transmitters that excludes D2D transmitter d_0^{Tx} with mmWave adversary a_0^{m} as the observation point (i.e., $\Phi_{\left\{\mathcal{D}^{\mathrm{Tx}}\setminus\left\{d_0^{\mathrm{Tx}}\right\}|a_0^{\mathrm{m}}\right\}}$). In contrast, if D2D transmitter d_0^{Tx} is active at mmWave communication mode (i.e., $\mathcal{D}_1\cap\mathcal{M}^{\mathrm{m}}$), the received signal power of mmWave adversary a_0^{m} will additionally include the signal power from D2D transmitter d_0^{Tx} (i.e., $y_{a_0^{\mathrm{m}}}=p^{\mathrm{D}}h^{\mathrm{m}}_{d_0^{\mathrm{Tx}}a_0^{\mathrm{m}}}g^{\mathrm{m}}_{d_0^{\mathrm{Tx}}a_0^{\mathrm{m}}}\ell^{\mathrm{m}}\left(\mathbf{x}_{d_0^{\mathrm{Tx}}},\mathbf{x}_{a_0^{\mathrm{m}}}\right)+I^{\mathrm{C}}_{a_0^{\mathrm{m}}}+I^{\mathrm{D}}_{a_0^{\mathrm{m}}}+N_{a_0^{\mathrm{m}}}$). In this case, mmWave adversary a_0^{m} can detect the transmission of D2D transmitter d_0^{Tx} according to its received signal power by using binary hypothesis testing [6], namely mmWave adversary a_0^{m} perceives event $\mathcal{D}_1\cap\mathcal{M}^{\mathrm{m}}$ ($\mathcal{D}_0\cup\left(\mathcal{D}_1\cap\mathcal{M}^{\mathrm{M}}\right)$) when $y_{a_0^{\mathrm{m}}}$ is larger (smaller) than a predefined threshold τ^{m} (i.e., $y_{a_0^{\mathrm{m}}}\underset{\mathcal{D}_1\cap\mathcal{M}^{\mathrm{m}}}{\overset{\mathcal{D}_0\cup\left(\mathcal{D}_1\cap\mathcal{M}^{\mathrm{M}}\right)}{\lessgtr}}\tau^{\mathrm{m}}$). In this framework, mmWave adversary a_0^{m} will make a False Alarm (FA) decision when $\mathcal{D}_0\cup\left(\mathcal{D}_1\cap\mathcal{M}^{\mathrm{M}}\right)$ happens while $y_{a_0^{\mathrm{m}}}>\tau^{\mathrm{m}}$. Moreover, mmWave adversary a_0^{m} will make a Miss Detection (MD) decision when $\mathcal{D}_1\cap\mathcal{M}^{\mathrm{m}}$ happens while $y_{a_0^{\mathrm{m}}}<\tau^{\mathrm{m}}$. The FA and MD probabilities of mmWave adversary a_0^{m} are

$$P^{\mathrm{FA}}_{a_0^{\mathrm{m}}}\left(p^{\mathrm{D}},p^{\mathcal{M}^{\mathrm{f}}},\tau^{\mathrm{m}}\right)=\mathbb{P}\left[y_{a_0^{\mathrm{m}}}>\tau^{\mathrm{m}}\middle|\,\mathcal{D}_0\cup\left(\mathcal{D}_1\cap\mathcal{M}^{\mathrm{M}}\right)\right]\tag{8}$$

and

$$P^{\mathrm{MD}}_{a_0^{\mathrm{m}}}\left(p^{\mathrm{D}},p^{\mathcal{M}^{\mathrm{f}}},\tau^{\mathrm{m}}\right)=\mathbb{P}\left[y_{a_0^{\mathrm{m}}}<\tau^{\mathrm{m}}\middle|\,\mathcal{D}_1\cap\mathcal{M}^{\mathrm{m}}\right],\tag{9}$$

the derivations of which are in Appendices D and E, and numerically verified in Figs. 3 and 4, respectively.

Similarly, the received signal power of microwave adversary a_0^{M} is $y_{a_0^{\mathrm{M}}}=I^{\mathrm{C}}_{a_0^{\mathrm{M}}}+I^{\mathrm{D}}_{a_0^{\mathrm{M}}}+N_{a_0^{\mathrm{M}}}$ if $\mathcal{D}_0\cup\left(\mathcal{D}_1\cap\mathcal{M}^{\mathrm{m}}\right)$ while $y_{a_0^{\mathrm{M}}}=p^{\mathrm{D}}h^{\mathrm{M}}_{d_0^{\mathrm{Tx}}a_0^{\mathrm{M}}}\ell^{\mathrm{M}}\left(\mathbf{x}_{d_0^{\mathrm{Tx}}},\mathbf{x}_{a_0^{\mathrm{M}}}\right)+I^{\mathrm{C}}_{a_0^{\mathrm{M}}}+I^{\mathrm{D}}_{a_0^{\mathrm{M}}}+N_{a_0^{\mathrm{M}}}$ if $\mathcal{D}_1\cap\mathcal{M}^{\mathrm{M}}$. Therein, $I^{\mathrm{C}}_{a_0^{\mathrm{M}}}=p^{\mathrm{M}}\sum_{b^{\mathrm{M}}\in\left\{\mathcal{B}^{\mathrm{M}}|a_0^{\mathrm{M}}\right\}}\mathbb{1}_{b^{\mathrm{M}}}h^{\mathrm{M}}_{b^{\mathrm{M}}a_0^{\mathrm{M}}}\ell^{\mathrm{M}}\left(\mathbf{x}_{b^{\mathrm{M}}},\mathbf{x}_{a_0^{\mathrm{M}}}\right)$ is the interference from microwave BSs, $I^{\mathrm{D}}_{a_0^{\mathrm{M}}}=p^{\mathrm{D}}\sum_{d^{\mathrm{Tx}}\in\left\{\mathcal{D}^{\mathrm{Tx}}\setminus\left\{d_0^{\mathrm{Tx}}\right\}|a_0^{\mathrm{m}}\right\}}\mathbb{1}_{d^{\mathrm{Tx}}}\left(1-\mathbb{1}^{\mathcal{M}^{\mathrm{m}}}_{d^{\mathrm{Tx}}}\right)h^{\mathrm{M}}_{d^{\mathrm{Tx}}a_0^{\mathrm{M}}}\ell^{\mathrm{M}}\left(\mathbf{x}_{d^{\mathrm{Tx}}},\mathbf{x}_{a_0^{\mathrm{M}}}\right)$ is that from D2D transmitters that are active at microwave communication mode, and $N_{a_0^{\mathrm{M}}}$ is the additive noise at microwave adversary a_0^{M}. Here, $\left\{\mathbf{x}_{b^{\mathrm{M}}}\right\}_{b^{\mathrm{M}}\in\left\{\mathcal{B}^{\mathrm{M}}|a_0^{\mathrm{M}}\right\}}$ is one of the realizations of the PP of

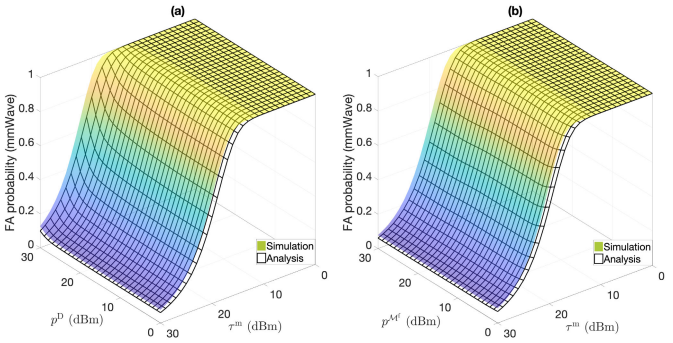

Fig. 3. Comparison between the simulation and analytical results on FA probability (mmWave) with (a) $p^{\mathcal{M}^{\mathrm{f}}} = 10\mathrm{dBm}$ and (b) $p^{\mathrm{D}} = 20\mathrm{dBm}$.

microwave BSs with microwave adversary a_0^{M} as the observation point (i.e., $\Phi_{\left\{\mathcal{B}^{\mathrm{M}}|a_0^{\mathrm{M}}\right\}}$) and $\left\{\mathbf{x}_{d^{\mathrm{Tx}}}\right\}_{d^{\mathrm{Tx}}\in\left\{\mathcal{D}^{\mathrm{Tx}}\setminus\left\{d_0^{\mathrm{Tx}}\right\}|a_0^{\mathrm{M}}\right\}}$ is that of D2D transmitters that excludes D2D transmitter d_0^{Tx} with microwave adversary a_0^{M} as the observation point (i.e., $\Phi_{\left\{\mathcal{D}^{\mathrm{Tx}}\setminus\left\{d_0^{\mathrm{Tx}}\right\}|a_0^{\mathrm{M}}\right\}}$). The FA and MD probabilities of microwave adversary a_0^{M} are

$$P_{a_0^{\mathrm{M}}}^{\mathrm{FA}}\left(p^{\mathrm{D}}, p^{\mathcal{M}^{\mathrm{f}}}, \tau^{\mathrm{M}}\right) = \mathbb{P}\left[y_{a_0^{\mathrm{M}}} > \tau^{\mathrm{M}} \middle| \mathcal{D}_0 \cup \left(\mathcal{D}_1 \cap \mathcal{M}^{\mathrm{m}}\right)\right] \tag{10}$$

and

$$P_{a_0^{\mathrm{M}}}^{\mathrm{MD}}\left(p^{\mathrm{D}}, p^{\mathcal{M}^{\mathrm{f}}}, \tau^{\mathrm{M}}\right) = \mathbb{P}\left[y_{a_0^{\mathrm{M}}} < \tau^{\mathrm{M}} \middle| \mathcal{D}_1 \cap \mathcal{M}^{\mathrm{M}}\right], \tag{11}$$

the derivations of which are in Appendices F and G, and numerically verified in Figs. 5 and 6, respectively.

IV. Formulation of Combat Game and Solution Design

A. Problem Formulation

In the network, the D2D users make decision on their transmission power and communication mode first while adversaries decide the detection threshold according to their received signal powers later. In this case, the decision-making of the D2D users is prior to that of the adversaries. This can be captured by using the framework of a two-stage Stackelberg game, where: 1) the adversaries are the followers aiming to minimize their detection errors at the lower stage, and their decisions on the predefined power threshold are the best response from the lower stage; and 2) the D2D users are the leaders at the upper stage aiming to maximize their utilities subject to the constraints on communication covertness and taking into account the best response from the lower stage. Specifically, the game formulation over the representative network nodes (i.e., microwave adversary a_0^{M}, mmWave adversary a_0^{m}, and typical D2D users) is a single-leader-two-followers game as follows:

1) *Lower Stage:* As the communication becomes covert when either FA or MD happens, the detection error probability of microwave adversary a_0^{M} can be defined as follows:

$$\left(\mathbb{P}^{\mathcal{D}_0} + \mathbb{P}^{\mathcal{D}_1}\mathbb{P}^{\mathcal{M}^{\mathrm{m}}}\right) P_{a_0^{\mathrm{M}}}^{\mathrm{FA}}\left(p^{\mathrm{D}}, p^{\mathcal{M}^{\mathrm{f}}}, \tau^{\mathrm{M}}\right) + \mathbb{P}^{\mathcal{D}_1}\mathbb{P}^{\mathcal{M}^{\mathrm{M}}} P_{a_0^{\mathrm{M}}}^{\mathrm{MD}}\left(p^{\mathrm{D}}, p^{\mathcal{M}^{\mathrm{f}}}, \tau^{\mathrm{M}}\right), \tag{15}$$

where $P_{a_0^{\mathrm{M}}}^{\mathrm{FA}}(\cdot,\cdot,\cdot)$ and $P_{a_0^{\mathrm{M}}}^{\mathrm{MD}}(\cdot,\cdot,\cdot)$ are defined in (10) and (11), respectively. However, as microwave adversary a_0^{M} is unaware of the probabilities of the events that D2D transmitter d_0^{Tx} is active at microwave communication mode and that is either mute or active at mmWave communication mode (i.e., $\mathbb{P}^{\mathcal{D}_1}\mathbb{P}^{\mathcal{M}^{\mathrm{M}}}$ and $\mathbb{P}^{\mathcal{D}_0} + \mathbb{P}^{\mathcal{D}_1}\mathbb{P}^{\mathcal{M}^{\mathrm{m}}}$, respectively), we omit these event probabilities and let microwave adversary a_0^{M} minimize its detection error[4]

$$\tau^{\mathrm{M}\star} = \arg\min_{\tau^{\mathrm{M}}} P_{a_0^{\mathrm{M}}}^{\mathrm{FA}}\left(p^{\mathrm{D}}, p^{\mathcal{M}^{\mathrm{f}}}, \tau^{\mathrm{M}}\right) + P_{a_0^{\mathrm{M}}}^{\mathrm{MD}}\left(p^{\mathrm{D}}, p^{\mathcal{M}^{\mathrm{f}}}, \tau^{\mathrm{M}}\right). \tag{16}$$

Moreover, this is to equivalently treat FA and MD so as to avoid any bias between them, which has been widely adopted in signal sensing area [28]. Furthermore, the detection error defined in (16) is an upper bound of the detection error probability defined in (15), which can be expressed in (12), shown at the bottom of the previous page.

Similarly, mmWave adversary a_0^{m} aims to minimize its own detection error as follows:

$$\tau^{\mathrm{m}\star} = \arg\min_{\tau^{\mathrm{m}}} P_{a_0^{\mathrm{m}}}^{\mathrm{FA}}\left(p^{\mathrm{D}}, p^{\mathcal{M}^{\mathrm{f}}}, \tau^{\mathrm{m}}\right) + P_{a_0^{\mathrm{m}}}^{\mathrm{MD}}\left(p^{\mathrm{D}}, p^{\mathcal{M}^{\mathrm{f}}}, \tau^{\mathrm{m}}\right), \tag{17}$$

where $P_{a_0^{\mathrm{m}}}^{\mathrm{FA}}(\cdot,\cdot,\cdot)$ and $P_{a_0^{\mathrm{m}}}^{\mathrm{MD}}(\cdot,\cdot,\cdot)$ are defined in (8) and (9), respectively.

2) *Upper Stage:* The problem of the typical D2D users is in (13), shown at the bottom of the previous page. Therein, the objective (i.e., (13a)) is the reward achieved by guaranteeing the link reliability of the hybrid D2D communication (i.e., gaining $u^{\mathrm{P,M}}$ if $\mathrm{SINR}_{d_0^{\mathrm{Rx}}}^{\mathrm{m}} \geq \eta^{\mathrm{m}}$ at the mmWave communication mode $\mathcal{M}^{\mathrm{m}}$ and $u^{\mathrm{P,m}}$ if $\mathrm{SINR}_{d_0^{\mathrm{Rx}}}^{\mathrm{M}} \geq \eta^{\mathrm{M}}$ at the microwave communication mode $\mathcal{M}^{\mathrm{M}}$) minusing the power cost (i.e., $u^{\mathrm{C}}p^{\mathrm{D}}$), where u^{C} is the unit cost. The constraints (i.e., (13b)) are to lower bound the detection error for both the microwave and mmWave adversaries so as to ensure a certain level of communication covertness (i.e., $1-\varepsilon$) for the hybrid D2D communication. $\underline{p^{\mathrm{D}}}$ and $\overline{p^{\mathrm{D}}}$ are the lower and upper bounds of the D2D transmission power p^{D}, respectively.

B. Solution Design

Given the D2D transmission power p^{D} and power threshold for switching communication mode $p^{\mathcal{M}^{\mathrm{f}}}$, we analyze the problem of microwave adversary a_0^{M} (i.e., (16)) and that of mmWave adversary a_0^{m} (i.e., (17)) can be done similarly. Specifically, the detection error of microwave adversary a_0^{M} can be rewritten in (14), shown at the bottom of the previous page. Therein, since $F_{p^{\mathrm{D}}h_{d_0^{\mathrm{Tx}}a_0^{\mathrm{M}}}^{\mathrm{M}}\ell^{\mathrm{M}}\left(\mathbf{x}_{d_0^{\mathrm{Tx}}},\mathbf{x}_{a_0^{\mathrm{M}}}\right)}(\cdot) \in [0,1]$, term (a) increases faster than term (b) With Respect To

[4]As pointed out in [25], [26], and [27], the D2D user can effectively ensure the adversary's inability to effectively carry out their detection attempts by establishing a lower bound on the sum of the probabilities of FA and MD with $1-\varepsilon$.

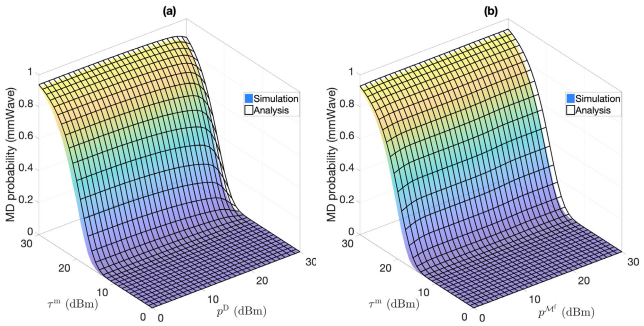

Fig. 4. Comparison between the simulation and analytical results on MD probability (mmWave) with (a) $p^{\mathcal{M}^{\mathrm{f}}} = 10\mathrm{dBm}$ and (b) $p^{\mathrm{D}} = 20\mathrm{dBm}$.

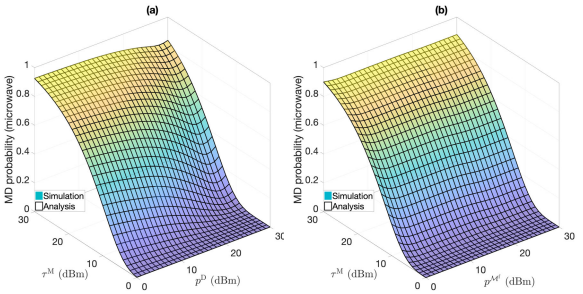

Fig. 6. Comparison between the simulation and analytical results on MD probability (microwave) with (a) $p^{\mathcal{M}^{\mathrm{f}}} = 10\mathrm{dBm}$ and (b) $p^{\mathrm{D}} = 20\mathrm{dBm}$.

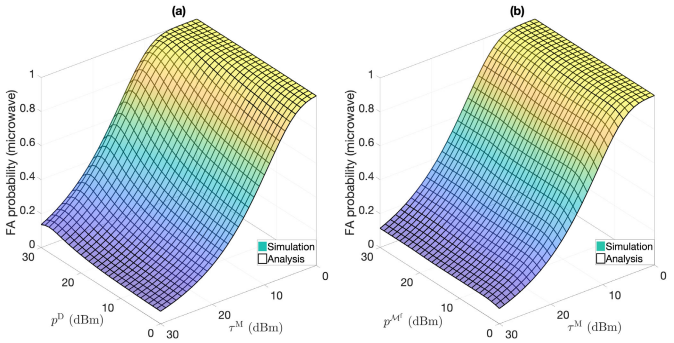

Fig. 5. Comparison between the simulation and analytical results on FA probability (microwave) with (a) $p^{\mathcal{M}^{\mathrm{f}}} = 10\mathrm{dBm}$ and (b) $p^{\mathrm{D}} = 20\mathrm{dBm}$.

(w.r.t.) τ^{M}, which can be verified in Fig. 7(b) when $\tau^{\mathrm{M}} \lessapprox 14\mathrm{dBm}$. As such, $P^{\mathrm{FA}}_{a_0^{\mathrm{M}}}\left(p^{\mathrm{D}}, p^{\mathcal{M}^{\mathrm{f}}}, \tau^{\mathrm{M}}\right) + P^{\mathrm{MD}}_{a_0^{\mathrm{M}}}\left(p^{\mathrm{D}}, p^{\mathcal{M}^{\mathrm{f}}}, \tau^{\mathrm{M}}\right)$ will decrease w.r.t. τ^{M} first. Later, when τ^{M} becomes larger (e.g., $\tau^{\mathrm{M}} = 30\mathrm{dBm}$), term (a) approaches its upper bound (i.e., 1) and thereby its increasing speed w.r.t. τ^{M} slows down and becomes slower than that of term (b). In this case, $P^{\mathrm{FA}}_{a_0^{\mathrm{M}}}\left(p^{\mathrm{D}}, p^{\mathcal{M}^{\mathrm{f}}}, \tau^{\mathrm{M}}\right) + P^{\mathrm{MD}}_{a_0^{\mathrm{M}}}\left(p^{\mathrm{D}}, p^{\mathcal{M}^{\mathrm{f}}}, \tau^{\mathrm{M}}\right)$ will increase w.r.t. τ^{M}, which can be observed in Fig. 7(b) when $\tau^{\mathrm{M}} \gtrapprox 14\mathrm{dBm}$. Consequently, $P^{\mathrm{FA}}_{a_0^{\mathrm{M}}}\left(p^{\mathrm{D}}, p^{\mathcal{M}^{\mathrm{f}}}, \tau^{\mathrm{M}}\right) + P^{\mathrm{MD}}_{a_0^{\mathrm{M}}}\left(p^{\mathrm{D}}, p^{\mathcal{M}^{\mathrm{f}}}, \tau^{\mathrm{M}}\right)$ is in trough shape w.r.t. τ^{M}, which induces a global minimal detection error marked by red pentagram in Fig. 7(b). Mathematically, finding such a global minimum in a trough-shape objective is a one-dimension search problem, which can be effectively and efficiently solved by one-dimension search methods, such as golden section search [29]. The gradient-based optimization method such as Newton method is inapplicable here due to that it is difficult to analyze the properties of the first and second-order derivatives of the detection error w.r.t. τ^{M}. τ^{M} corresponding to the global minimal detection error is the best response of the lower stage.

Taking into account the best response of the lower stage, the problem of the D2D users defined in (13) is a constrained bi-level optimization problem. Due to the multi-integral terms in both the objective and constraints of (13), it is difficult to analyze the convexity of (13) and, hence, conventional convex optimization is inapplicable. In this case, we resort to non-convex optimization method and adopt the bi-level algorithm in [4], which is developed based on successive convex approximation, to solve (13). The complexity and convergence of the bi-level algorithm have been discussed in [30].

$$\begin{aligned}&\left(\mathbb{P}^{\mathcal{D}_0} + \mathbb{P}^{\mathcal{D}_1}\mathbb{P}^{\mathcal{M}^{\mathrm{m}}}\right) P^{\mathrm{FA}}_{a_0^{\mathrm{M}}}\left(p^{\mathrm{D}}, p^{\mathcal{M}^{\mathrm{f}}}, \tau^{\mathrm{M}}\right) + \mathbb{P}^{\mathcal{D}_1}\mathbb{P}^{\mathcal{M}^{\mathrm{M}}} P^{\mathrm{MD}}_{a_0^{\mathrm{M}}}\left(p^{\mathrm{D}}, p^{\mathcal{M}^{\mathrm{f}}}, \tau^{\mathrm{M}}\right)\\ &\quad\le \underbrace{\max\left\{\mathbb{P}^{\mathcal{D}_1}\mathbb{P}^{\mathcal{M}^{\mathrm{M}}}, \mathbb{P}^{\mathcal{D}_0} + \mathbb{P}^{\mathcal{D}_1}\mathbb{P}^{\mathcal{M}^{\mathrm{m}}}\right\}}_{\le 1}\left[P^{\mathrm{FA}}_{a_0^{\mathrm{M}}}\left(p^{\mathrm{D}}, p^{\mathcal{M}^{\mathrm{f}}}, \tau^{\mathrm{M}}\right) + P^{\mathrm{MD}}_{a_0^{\mathrm{M}}}\left(p^{\mathrm{D}}, p^{\mathcal{M}^{\mathrm{f}}}, \tau^{\mathrm{M}}\right)\right].\end{aligned} \tag{12}$$

$$\max_{p^{\mathrm{D}},\, p^{\mathcal{M}^{\mathrm{f}}} \in \left[\underline{p^{\mathrm{D}}},\, \overline{p^{\mathrm{D}}}\right]} \; u^{\mathrm{P,M}}\mathbb{P}\left[\mathrm{SINR}^{\mathrm{M}}_{d_0^{\mathrm{Rx}}} \ge \eta^{\mathrm{M}} \middle| \mathcal{D}_1 \cap \mathcal{M}^{\mathrm{M}}\right]\mathbb{P}^{\mathcal{M}^{\mathrm{M}}} + u^{\mathrm{P,m}}\mathbb{P}\left[\mathrm{SINR}^{\mathrm{m}}_{d_0^{\mathrm{Rx}}} \ge \eta^{\mathrm{m}} \middle| \mathcal{D}_1 \cap \mathcal{M}^{\mathrm{m}}\right]\mathbb{P}^{\mathcal{M}^{\mathrm{m}}} - u^{\mathrm{C}}p^{\mathrm{D}} \tag{13a}$$

$$\text{s.t. } P^{\mathrm{FA}}_{a_0^{\mathrm{f}}}\left(p^{\mathrm{D}}, p^{\mathcal{M}^{\mathrm{f}}}, \tau^{\mathrm{f}\star}\right) + P^{\mathrm{MD}}_{a_0^{\mathrm{f}}}\left(p^{\mathrm{D}}, p^{\mathcal{M}^{\mathrm{f}}}, \tau^{\mathrm{f}\star}\right) \ge 1 - \varepsilon,\ \forall f \in \{\mathrm{M}, \mathrm{m}\}. \tag{13b}$$

$$\begin{aligned}&P^{\mathrm{FA}}_{a_0^{\mathrm{M}}}\left(p^{\mathrm{D}}, p^{\mathcal{M}^{\mathrm{f}}}, \tau^{\mathrm{M}}\right) + P^{\mathrm{MD}}_{a_0^{\mathrm{M}}}\left(p^{\mathrm{D}}, p^{\mathcal{M}^{\mathrm{f}}}, \tau^{\mathrm{M}}\right)\\ &= 1 - \underbrace{\int_0^{\tau^{\mathrm{M}} - N_{a_0^{\mathrm{M}}}} f_{I^{\mathrm{C}}_{a_0^{\mathrm{M}}} + I^{\mathrm{D}}_{a_0^{\mathrm{M}}}}(t)\,\mathrm{d}t}_{(a)} + \underbrace{\int_0^{\tau^{\mathrm{M}} - N_{a_0^{\mathrm{M}}}} F_{p^{\mathrm{D}} h^{\mathrm{M}}_{d_0^{\mathrm{Tx}} a_0^{\mathrm{M}}} \ell^{\mathrm{M}}\left(\mathbf{x}_{d_0^{\mathrm{Tx}}}, \mathbf{x}_{a_0^{\mathrm{M}}}\right)}\left(\tau^{\mathrm{M}} - N_{a_0^{\mathrm{M}}} - t\right) f_{I^{\mathrm{C}}_{a_0^{\mathrm{M}}} + I^{\mathrm{D}}_{a_0^{\mathrm{M}}}}(t)\,\mathrm{d}t}_{(b)}.\end{aligned} \tag{14}$$

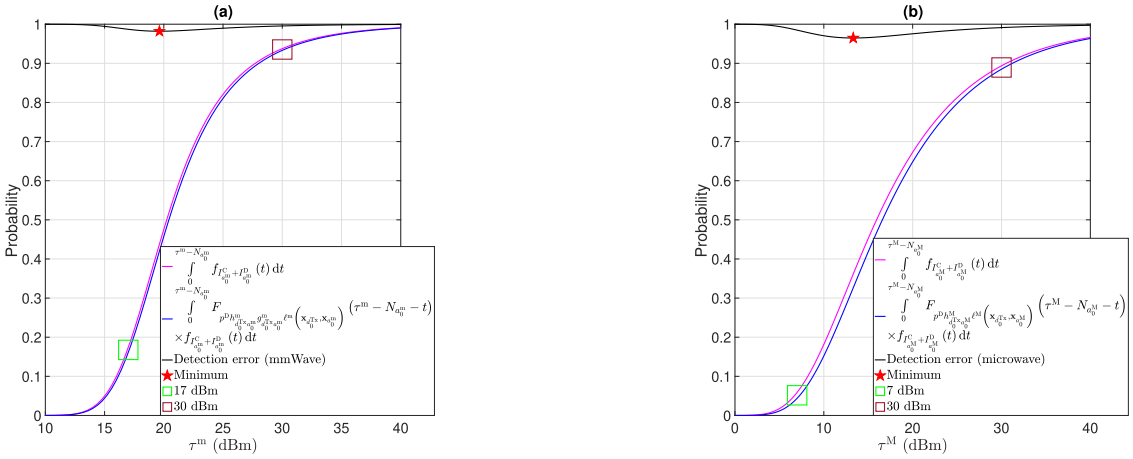

Fig. 7. Characteristics of the problem of (a) mmWave and (b) microwave adversaries with $p^{\mathcal{M}^{\mathrm{f}}} = 10\mathrm{dBm}$ and $p^{\mathrm{D}} = 20\mathrm{dBm}$.

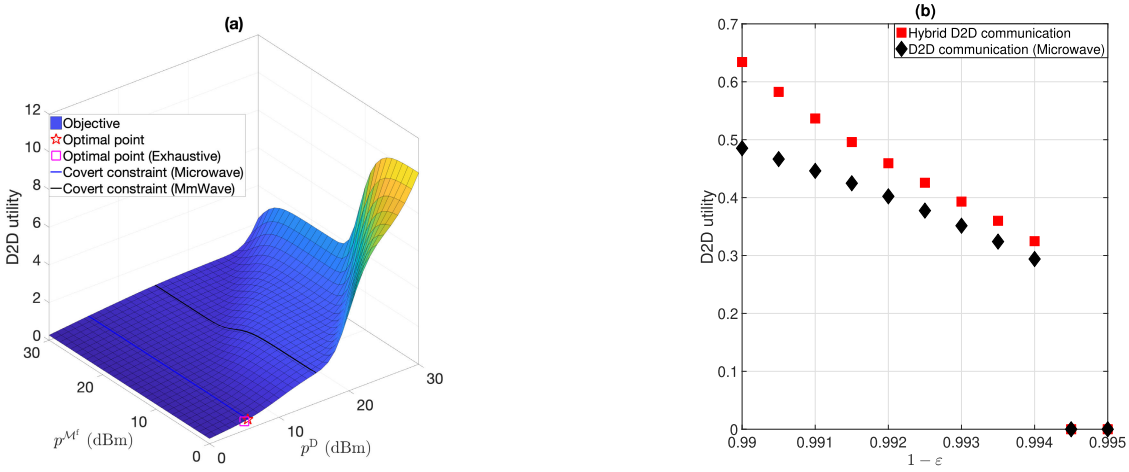

Fig. 8. (a) Stackelberg equilibrium and (b) hybrid D2D communication or conventional D2D communication?

V. Performance Evaluation

In this section, we present numerical results to evaluate the performance of the Stackelberg game formulated in Section IV-A. The parameter setting is in Table I together with the corresponding physical meaning. First, we verify the optimality of the obtained equilibrium by comparing it with the equilibrium obtained by exhaustive search in Fig. 8(a). Then, we demonstrate the advantages of the hybrid D2D communication by comparing it with the conventional D2D communication in Fig. 8(b). We demonstrate the effectiveness of cellular signal in enhancing communication covertness for D2D communication in Fig. 9(a). Moreover, we study the role of D2D communication distance in avoiding transmission detection in Fig. 9(b). Furthermore, we evaluate the impact of decoding threshold on system performance in Fig. 9(c).

Figure 8(a) depicts the D2D utility as a function of the D2D transmission power p^{D} and power threshold for switching communication mode $p^{\mathcal{M}^{\mathrm{f}}}$. In Fig. 8(a), we can observe that the optimal strategy (i.e., optimal D2D transmission power and power threshold for switching communication mode) can maximize the D2D utility within the feasible domain. Therein, the feasible domain is determined by the constraints on communication covertness (i.e., (13b)). The optimal strategy is obtained by the bi-level optimization algorithm developed in [4] and is consistent with that obtained by the exhaustive search, which validates the optimality of the obtained optimal strategy. This together with the existence and uniqueness of the adversaries' responses verified in Fig. 7 implies the optimality of the Stackelberg equilibrium, where the Stackelberg equilibrium constitutes the obtained optimal strategy of the D2D users and the corresponding responses from the adversaries. Moreover, as observed in Fig. 8(a), the constraint on communication covertness over the microwave frequency band requires the D2D transmission power $p^{\mathrm{D}} \lessapprox 5\mathrm{dBm}$ while that over the mmWave frequency band requires $p^{\mathrm{D}} \lessapprox 18\mathrm{dBm}$. The reason is that the signal power leaked to the mmWave adversaries is tiny as beamforming is adopted for mmWave communication. In contrast, the signal over the microwave frequency band propagates on a free-space manner, which implies high signal power leaked to the microwave adversaries.

Figure 8(b) demonstrates the advantages of hybrid D2D communication over conventional D2D communication (i.e., D2D communication over microwave frequency band). As shown in Fig. 8(b), the D2D utility decreases as the constraint of communication covertness becomes tighter and finally becomes 0 when detection error $1-\varepsilon \geq 0.9945$ due

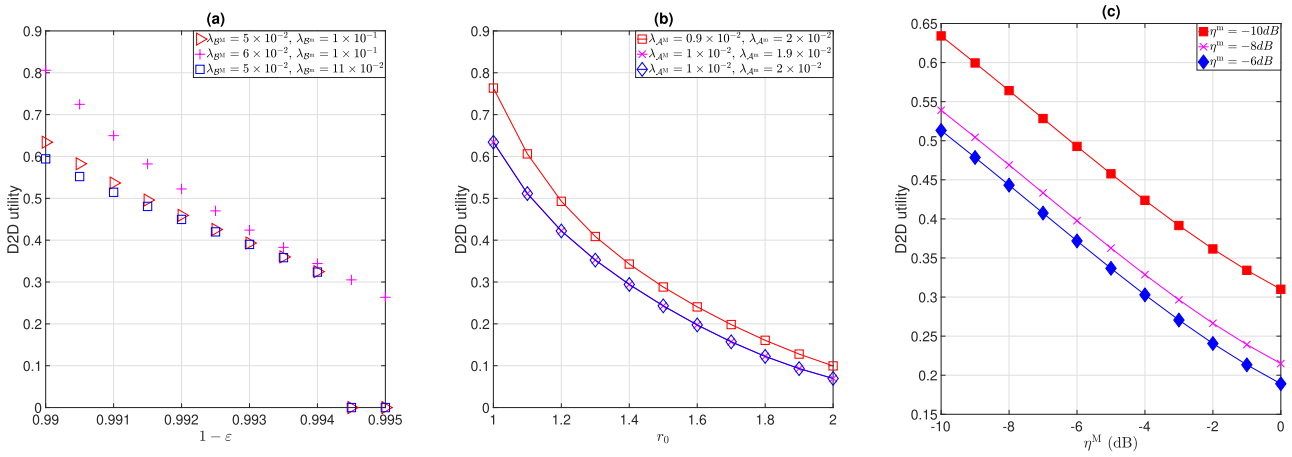

Fig. 9. Impacts of (a) density of BSs, (b) D2D communication distance, and (c) decoding threshold.

to the unsatisfied constraints on communication covertness (i.e., (13b)). Therein, the D2D utility obtained by the hybrid D2D communication is higher than that obtained by the conventional D2D communication, which demonstrates the advantage of hybrid D2D communication over the conventional D2D communication regarding throughput. However, the decreasing rate of the D2D utility obtained by the hybrid D2D communication w.r.t. $1-\varepsilon$ is faster than that obtained by the conventional D2D communication. The reason can be explained as follows. The high throughout of hybrid D2D communication is mostly achieved by its mmWave communication. With tighter constraints on communication covertness, the D2D transmission power has to be gradually reduced, and the blockage effect of mmwWave communication of hybrid D2D communication becomes severe. By such, the conventional D2D communication outperforms the hybrid D2D communication regarding the resistance to more stringent security requirement.

Figure 9(a) evaluates the impact of the density of the BSs on the D2D utility. We can observe that the increase in the density of microwave BSs can make the D2D utility nonzero when $1-\varepsilon \geq 0.9945$. The reason can be explained as follows. The increase in the density of microwave BSs can increase the interference dynamics at the microwave adversaries and further improve the communication covertness of D2D transmission over the microwave frequency band. In this case, the constraint on communication covertness over microwave frequency band can be loosen (see Fig. 8(a)), and a nonzero D2D utility is achievable when $1-\varepsilon \geq 0.9945$.

Figure 9(b) evaluates the impact of D2D communication distance on the D2D utility. As observed, the decrease in the density of mmWave adversaries does not affect the D2D utility while that of microwave adversaries improves the D2D utility. The reason has been given in the discussion of Fig. 9(a). Additionally, the D2D utility decreases as the D2D communication distance increases. The reason can be explained as follows. The link reliability of D2D transmission weakens as the D2D communication distance increases. To enhance the link reliability of D2D transmission, we have to increase the D2D transmission power, which, however, make it easier for the adversaries to detect D2D transmission. This implies that by shortening D2D communication distance, both the link reliability and communication covertness can be improved.

Figure 9(c) depicts the D2D utility as a function of the decoding threshold over microwave frequency band η^{M}. The D2D utility convexly decreases as η^{M} increases. This is due to that the successful transmission probability over microwave frequency band (i.e., (7)) gradually approaches its lower bound, and its decreasing rate slows down, which induces a convex decreasing trend for the D2D utility.

VI. Conclusion

We have implemented covert communication techniques to enhance the security of the hybrid D2D communication within a large-scale D2D-underlaid cellular network, aiming to mitigate the risk of detection by adversaries. Our objective is to improve link reliability while adhering to the constraint of communication covertness. To analyze the network performance from a system-level perspective, we utilize stochastic geometry to model the geographical configuration of the network. We employ a two-stage Stackelberg game framework to conceptualize the strategic interaction between D2D users and adversaries and thereby capture their conflict of interests. Here, adversaries act as followers at the lower stage, while D2D users take on the role of leaders at the upper stage. For the adversary's problem, we verify the existence and uniqueness of their optimal strategy, deriving it as the best response from the lower stage. Incorporating this best response, we employ a bi-level algorithm to solve the problem and determine the optimal strategy for D2D users. This, along with the adversary's strategy, forms the Stackelberg equilibrium. We rigorously verify the optimality of this equilibrium. Numerical results have been presented and interesting insights have been discussed, including

- Hybrid D2D communication shows advantages over conventional D2D communication regarding the D2D utility under the same constraint on communication covertness, as elucidated in the discussion of Fig. 8(b).
- Decreasing the communication distance between the D2D users can improve both the utility and communication covertness for the D2D users, as illustrated in the discussion of Fig. 9(b).

$$\begin{aligned}
&\mathbb{P}\left[\mathrm{SINR}_{d_0^{\mathrm{Rx}}}^{\mathrm{m}} \geq \eta^{\mathrm{m}} \middle| \mathcal{D}_1 \cap \mathcal{M}^{\mathrm{m}}\right] \\
&= \mathbb{P}\left[\frac{p^{\mathrm{D}} h_{d_0^{\mathrm{Tx}} d_0^{\mathrm{Rx}}}^{\mathrm{m}} g_{d_0^{\mathrm{Tx}} d_0^{\mathrm{Rx}}}^{\mathrm{m}} \ell^{\mathrm{m}}\left(\mathbf{x}_{d_0^{\mathrm{Tx}}}, \mathbf{x}_{d_0^{\mathrm{Rx}}}\right)}{I_{d_0^{\mathrm{Rx}}}^{\mathrm{C},\mathrm{m}} + I_{d_0^{\mathrm{Rx}}}^{\mathrm{D},\mathrm{m}} + N_{d_0^{\mathrm{Rx}}}^{\mathrm{m}}} \geq \eta^{\mathrm{m}}\right] \\
&\overset{(2)}{=} \sum_{\substack{\mathrm{g}\in\mathcal{G} \\ \mathrm{s}\in\mathcal{S}}} \mathbb{P}^{g_{\mathcal{D}^{\mathrm{Tx}}\mathcal{D}^{\mathrm{Rx}}}^{\mathrm{g}}} P^{\mathrm{s}}(r_0)\, \mathbb{P}\left[h_{d_0^{\mathrm{Tx}} d_0^{\mathrm{Rx}}}^{\mathrm{m}} \geq \frac{\eta^{\mathrm{m}} r_0^{\alpha^{\mathrm{m},\mathrm{s}}}}{p^{\mathrm{D}} g_{\mathcal{D}^{\mathrm{Tx}}\mathcal{D}^{\mathrm{Rx}}}^{\mathrm{g}}}\left(I_{d_0^{\mathrm{Rx}}}^{\mathrm{C},\mathrm{m}} + I_{d_0^{\mathrm{Rx}}}^{\mathrm{D},\mathrm{m}} + N_{d_0^{\mathrm{Rx}}}^{\mathrm{m}}\right) \middle| \mathrm{s}\right]. \qquad (18)
\end{aligned}$$

$$\begin{aligned}
&\mathbb{P}\left[h_{d_0^{\mathrm{Tx}} d_0^{\mathrm{Rx}}}^{\mathrm{m}} \geq \frac{\eta^{\mathrm{m}} r_0^{\alpha^{\mathrm{m},\mathrm{s}}}}{p^{\mathrm{D}} g_{\mathcal{D}^{\mathrm{Tx}}\mathcal{D}^{\mathrm{Rx}}}^{\mathrm{g}}}\left(I_{d_0^{\mathrm{Rx}}}^{\mathrm{C},\mathrm{m}} + I_{d_0^{\mathrm{Rx}}}^{\mathrm{D},\mathrm{m}} + N_{d_0^{\mathrm{Rx}}}^{\mathrm{m}}\right) \middle| \mathrm{s}\right] \overset{(a)}{\leq} 1 - \mathbb{E}_{I_{d_0^{\mathrm{Rx}}}^{\mathrm{C},\mathrm{m}} + I_{d_0^{\mathrm{Rx}}}^{\mathrm{D},\mathrm{m}}}\left[\left(1 - \exp\left(-\iota\left(I_{d_0^{\mathrm{Rx}}}^{\mathrm{C},\mathrm{m}} + I_{d_0^{\mathrm{Rx}}}^{\mathrm{D},\mathrm{m}} + N_{d_0^{\mathrm{Rx}}}^{\mathrm{m}}\right)\right)\right)^{\upsilon^{\mathrm{s}}}\right] \\
&\overset{(b)}{=} \sum_{\upsilon=1}^{\upsilon^{\mathrm{s}}} \binom{\upsilon^{\mathrm{s}}}{\upsilon} (-1)^{\upsilon+1} \exp\left(-\upsilon\iota N_{d_0^{\mathrm{Rx}}}^{\mathrm{m}}\right) \mathbb{E}_{I_{d_0^{\mathrm{Rx}}}^{\mathrm{C},\mathrm{m}}}\left[\exp\left(-\upsilon\iota I_{d_0^{\mathrm{Rx}}}^{\mathrm{C},\mathrm{m}}\right)\right] \mathbb{E}_{I_{d_0^{\mathrm{Rx}}}^{\mathrm{D},\mathrm{m}}}\left[\exp\left(-\upsilon\iota I_{d_0^{\mathrm{Rx}}}^{\mathrm{D},\mathrm{m}}\right)\right]. \qquad (19)
\end{aligned}$$

$$\begin{aligned}
&\mathbb{E}_{h_{b^{\mathrm{m}} d_0^{\mathrm{Rx}}}^{\mathrm{m}}}\left[\exp\left(-\upsilon\iota p^{\mathrm{m}} h_{b^{\mathrm{m}} d_0^{\mathrm{Rx}}}^{\mathrm{m}} g_{\mathcal{B}^{\mathrm{m}}\mathcal{D}^{\mathrm{Rx}}}^{\mathrm{g}} \ell^{\mathrm{m}}\left(\mathbf{x}_{b^{\mathrm{m}}}, \mathbf{x}_{d_0^{\mathrm{Rx}}}\right)\right)\right] \\
&= \sum_{\mathrm{s}\in\mathcal{S}} P^{\mathrm{s}}\left(r_{b^{\mathrm{m}} d_0^{\mathrm{Rx}}}\right) \int_0^{+\infty} \exp\left(-\upsilon\iota p^{\mathrm{m}} h g_{\mathcal{B}^{\mathrm{m}}\mathcal{D}^{\mathrm{Rx}}}^{\mathrm{g}} r_{b^{\mathrm{m}} d_0^{\mathrm{Rx}}}^{-\alpha^{\mathrm{m},\mathrm{s}}}\right) \frac{\exp\left(-h\upsilon^{\mathrm{s}}\right)\left(\upsilon^{\mathrm{s}} h\right)^{\upsilon^{\mathrm{s}}}}{\Gamma\left(\upsilon^{\mathrm{s}}\right) h} \mathrm{d}h \\
&= \sum_{\mathrm{s}\in\mathcal{S}} P^{\mathrm{s}}\left(r_{b^{\mathrm{m}} d_0^{\mathrm{Rx}}}\right) \frac{\left(\upsilon^{\mathrm{s}}\right)^{\upsilon^{\mathrm{s}}}}{\Gamma\left(\upsilon^{\mathrm{s}}\right)} \int_0^{+\infty} \exp\left(-\left(\upsilon\iota p^{\mathrm{m}} g_{\mathcal{B}^{\mathrm{m}}\mathcal{D}^{\mathrm{Rx}}}^{\mathrm{g}} r_{b^{\mathrm{m}} d_0^{\mathrm{Rx}}}^{-\alpha^{\mathrm{m},\mathrm{s}}} + \upsilon^{\mathrm{s}}\right) h\right) h^{\upsilon^{\mathrm{s}}-1} \mathrm{d}h = \sum_{\mathrm{s}\in\mathcal{S}} \frac{P^{\mathrm{s}}\left(r_{b^{\mathrm{m}} d_0^{\mathrm{Rx}}}\right)}{\left(\frac{\upsilon\iota p^{\mathrm{m}}}{\upsilon^{\mathrm{s}}} g_{\mathcal{B}^{\mathrm{m}}\mathcal{D}^{\mathrm{Rx}}}^{\mathrm{g}} r_{b^{\mathrm{m}} d_0^{\mathrm{Rx}}}^{-\alpha^{\mathrm{m},\mathrm{s}}} + 1\right)^{\upsilon^{\mathrm{s}}}}. \qquad (20)
\end{aligned}$$

$$\begin{aligned}
&\mathbb{E}_{I_{d_0^{\mathrm{Rx}}}^{\mathrm{C},\mathrm{m}}}\left[\exp\left(-\upsilon\iota I_{d_0^{\mathrm{Rx}}}^{\mathrm{C},\mathrm{m}}\right)\right] = \mathbb{E}_{\Phi_{\left\{\mathcal{B}^{\mathrm{m}} | d_0^{\mathrm{Rx}}\right\}}}\left[\prod_{b^{\mathrm{m}}\in\left\{\mathcal{B}^{\mathrm{m}} | d_0^{\mathrm{Rx}}\right\}}\left[\mathbb{P}^{\mathcal{C}_0^{\mathrm{m}}} + \mathbb{P}^{\mathcal{C}_1^{\mathrm{m}}} \sum_{\substack{\mathrm{g}\in\mathcal{G} \\ \mathrm{s}\in\mathcal{S}}} \frac{\mathbb{P}^{g_{\mathcal{B}^{\mathrm{m}}\mathcal{D}^{\mathrm{Rx}}}^{\mathrm{g}}} P^{\mathrm{s}}\left(r_{b^{\mathrm{m}} d_0^{\mathrm{Rx}}}\right)}{\left(\frac{\upsilon\iota p^{\mathrm{m}} g_{\mathcal{B}^{\mathrm{m}}\mathcal{D}^{\mathrm{Rx}}}^{\mathrm{g}} r_{b^{\mathrm{m}} d_0^{\mathrm{Rx}}}^{-\alpha^{\mathrm{m},\mathrm{s}}}}{\upsilon^{\mathrm{s}}} + 1\right)^{\upsilon^{\mathrm{s}}}}\right]\right] \\
&\overset{(a)}{=} \exp\left(-2\pi\lambda_{\mathcal{B}^{\mathrm{m}}} \mathbb{P}^{\mathcal{C}_1^{\mathrm{m}}} \int_0^{+\infty}\left[1 - \sum_{\substack{\mathrm{g}\in\mathcal{G} \\ \mathrm{s}\in\mathcal{S}} \frac{\mathbb{P}^{g_{\mathcal{B}^{\mathrm{m}}\mathcal{D}^{\mathrm{Rx}}}^{\mathrm{g}}} P^{\mathrm{s}}(r)}{\left(\frac{\upsilon\iota p^{\mathrm{m}} g_{\mathcal{B}^{\mathrm{m}}\mathcal{D}^{\mathrm{Rx}}}^{\mathrm{g}} r^{-\alpha^{\mathrm{m},\mathrm{s}}}}{\upsilon^{\mathrm{s}}} + 1\right)^{\upsilon^{\mathrm{s}}}}\right] r\mathrm{d}r\right) \\
&= \exp\left(-2\pi\lambda_{\mathcal{B}^{\mathrm{m}}} \mathbb{P}^{\mathcal{C}_1^{\mathrm{m}}} \sum_{\substack{\mathrm{g}\in\mathcal{G} \\ \mathrm{s}\in\mathcal{S}} \mathbb{P}^{g_{\mathcal{B}^{\mathrm{m}}\mathcal{D}^{\mathrm{Rx}}}^{\mathrm{g}}} \int_0^{+\infty} P^{\mathrm{s}}(r)\left[1 - \frac{1}{\left(\frac{\upsilon\iota p^{\mathrm{m}} g_{\mathcal{B}^{\mathrm{m}}\mathcal{D}^{\mathrm{Rx}}}^{\mathrm{g}} r^{-\alpha^{\mathrm{m},\mathrm{s}}}}{\upsilon^{\mathrm{s}}} + 1\right)^{\upsilon^{\mathrm{s}}}}\right] r\mathrm{d}r\right). \qquad (21)
\end{aligned}$$

$$\begin{aligned}
&\mathbb{P}_{a_0^{\mathrm{m}}}^{\mathrm{FA}}\left(p^{\mathrm{D}}, p^{\mathcal{M}^{\mathrm{f}}}, \tau^{\mathrm{m}}\right) = \mathbb{P}\left[y_{a_0^{\mathrm{m}}} > \tau^{\mathrm{m}} \middle| \mathcal{D}_0 \cup \left(\mathcal{D}_1 \cap \mathcal{M}^{\mathrm{M}}\right)\right] = \mathbb{P}\left[I_{a_0^{\mathrm{m}}}^{\mathrm{C}} + I_{a_0^{\mathrm{m}}}^{\mathrm{D}} + N_{a_0^{\mathrm{m}}} > \tau^{\mathrm{m}}\right] \\
&= 1 - F_{I_{a_0^{\mathrm{m}}}^{\mathrm{C}} + I_{a_0^{\mathrm{m}}}^{\mathrm{D}}}\left(\tau^{\mathrm{m}} - N_{a_0^{\mathrm{m}}}\right) \overset{(a)}{=} \mathbb{P}\left[\xi < \frac{I_{a_0^{\mathrm{m}}}^{\mathrm{C}} + I_{a_0^{\mathrm{m}}}^{\mathrm{D}}}{\tau^{\mathrm{m}} - N_{a_0^{\mathrm{m}}}}\right] \overset{(b)}{\approx} \mathbb{E}_{I_{a_0^{\mathrm{m}}}^{\mathrm{C}} + I_{a_0^{\mathrm{m}}}^{\mathrm{D}}}\left[\left(1 - \exp\left(-\iota\frac{I_{a_0^{\mathrm{m}}}^{\mathrm{C}} + I_{a_0^{\mathrm{m}}}^{\mathrm{D}}}{\tau^{\mathrm{m}} - N_{a_0^{\mathrm{m}}}}\right)\right)^N\right] \\
&= \mathbb{E}_{I_{a_0^{\mathrm{m}}}^{\mathrm{C}} + I_{a_0^{\mathrm{m}}}^{\mathrm{D}}}\left[\sum_{n=0}^{N} \binom{N}{n} (-1)^n \exp\left(-n\iota\frac{I_{a_0^{\mathrm{m}}}^{\mathrm{C}} + I_{a_0^{\mathrm{m}}}^{\mathrm{D}}}{\tau^{\mathrm{m}} - N_{a_0^{\mathrm{m}}}}\right)\right] = \sum_{n=0}^{N} \binom{N}{n} (-1)^n \mathbb{E}_{I_{a_0^{\mathrm{m}}}^{\mathrm{C}} + I_{a_0^{\mathrm{m}}}^{\mathrm{D}}}\left[\exp\left(-n\iota\frac{I_{a_0^{\mathrm{m}}}^{\mathrm{C}} + I_{a_0^{\mathrm{m}}}^{\mathrm{D}}}{\tau^{\mathrm{m}} - N_{a_0^{\mathrm{m}}}}\right)\right]. \qquad (22)
\end{aligned}$$

$$\begin{aligned}
&\mathbb{P}\left[\mathrm{SINR}_{d_0^{\mathrm{Rx}}}^{\mathrm{M}} \geq \eta^{\mathrm{M}} \middle| \mathcal{D}_1 \cap \mathcal{M}^{\mathrm{M}}\right] = \mathbb{P}\left[\frac{p^{\mathrm{D}} h_{d_0^{\mathrm{Tx}} d_0^{\mathrm{Rx}}}^{\mathrm{M}} \ell^{\mathrm{M}}\left(\mathbf{x}_{d_0^{\mathrm{Tx}}}, \mathbf{x}_{d_0^{\mathrm{Rx}}}\right)}{I_{d_0^{\mathrm{Rx}}}^{\mathrm{C},\mathrm{M}} + I_{d_0^{\mathrm{Rx}}}^{\mathrm{D},\mathrm{M}} + N_{d_0^{\mathrm{Rx}}}^{\mathrm{M}}} \geq \eta^{\mathrm{M}}\right] \\
&= \mathbb{P}\left[h_{d_0^{\mathrm{Tx}} d_0^{\mathrm{Rx}}}^{\mathrm{M}} \geq \frac{\eta^{\mathrm{M}} r_0^{\alpha^{\mathrm{M}}}}{p^{\mathrm{D}}}\left(I_{d_0^{\mathrm{Rx}}}^{\mathrm{C},\mathrm{M}} + I_{d_0^{\mathrm{Rx}}}^{\mathrm{D},\mathrm{M}} + N_{d_0^{\mathrm{Rx}}}^{\mathrm{M}}\right)\right] \\
&\overset{(a)}{=} \exp\left(-\frac{\eta^{\mathrm{M}} r_0^{\alpha^{\mathrm{M}}}}{p^{\mathrm{D}}} N_{d_0^{\mathrm{Rx}}}^{\mathrm{M}}\right) \mathbb{E}_{I_{d_0^{\mathrm{Rx}}}^{\mathrm{C},\mathrm{M}}}\left[\exp\left(-\frac{\eta^{\mathrm{M}} r_0^{\alpha^{\mathrm{M}}}}{p^{\mathrm{D}}} I_{d_0^{\mathrm{Rx}}}^{\mathrm{C},\mathrm{M}}\right)\right] \mathbb{E}_{I_{d_0^{\mathrm{Rx}}}^{\mathrm{D},\mathrm{M}}}\left[\exp\left(-\frac{\eta^{\mathrm{M}} r_0^{\alpha^{\mathrm{M}}}}{p^{\mathrm{D}}} I_{d_0^{\mathrm{Rx}}}^{\mathrm{D},\mathrm{M}}\right)\right], \qquad (23)
\end{aligned}$$

- The increase in the co-channel interference from cellular network can enhance the resistance of D2D users to the adversaries (see the discussion of Fig. 9(a).

For future work, we would like to investigate the combat between the D2D users and adversaries on a long-run manner.

Appendix A
Probability of Being Active at mmWave Communication Mode

According to (4), the probability that the typical users are active at mmWave communication mode is

$$\begin{aligned}&\mathbb{P}^{\mathcal{M}^{\mathrm{m}}}\\&=\mathbb{P}\left[p^{\mathrm{D}}h^{\mathrm{m}}_{d_0^{\mathrm{Tx}}d_0^{\mathrm{Rx}}}g^{\mathrm{m}}_{d_0^{\mathrm{Tx}}d_0^{\mathrm{Rx}}}\ell^{\mathrm{m}}\left(\mathbf{x}_{d_0^{\mathrm{Tx}}},\mathbf{x}_{d_0^{\mathrm{Rx}}}\right)\geq p^{\mathcal{M}^{\mathrm{f}}}\right]\\&=\sum_{\substack{\mathrm{g}\in\mathcal{G}\\\mathrm{s}\in\mathcal{S}}}\mathbb{P}^{g^{\mathrm{g}}_{\mathcal{D}^{\mathrm{Tx}}\mathcal{D}^{\mathrm{Rx}}}}P^{\mathrm{s}}\left(r_0\right)\mathbb{P}\left[h^{\mathrm{m}}_{d_0^{\mathrm{Tx}}d_0^{\mathrm{Rx}}}\geq\frac{p^{\mathcal{M}^{\mathrm{f}}}r_0^{\alpha^{\mathrm{m},\mathrm{s}}}}{p^{\mathrm{D}}g^{\mathrm{g}}_{\mathcal{D}^{\mathrm{Tx}}\mathcal{D}^{\mathrm{Rx}}}}\middle|\mathrm{s}\right]\\&=\sum_{\substack{\mathrm{g}\in\mathcal{G}\\\mathrm{s}\in\mathcal{S}}}\mathbb{P}^{g^{\mathrm{g}}_{\mathcal{D}^{\mathrm{Tx}}\mathcal{D}^{\mathrm{Rx}}}}P^{\mathrm{s}}\left(r_0\right)\left[1-F_{h^{\mathrm{m}}_{d_0^{\mathrm{Tx}}d_0^{\mathrm{Rx}}}}\left(\frac{p^{\mathcal{M}^{\mathrm{f}}}r_0^{\alpha^{\mathrm{m},\mathrm{s}}}}{p^{\mathrm{D}}g^{\mathrm{g}}_{\mathcal{D}^{\mathrm{Tx}}\mathcal{D}^{\mathrm{Rx}}}}\right)\right],\end{aligned}\tag{24}$$

where $F_{h^{\mathrm{m}}_{d_0^{\mathrm{Tx}}d_0^{\mathrm{Rx}}}}(\cdot)$ can be obtained according to (3).

Appendix B
SINR Distribution of D2D Communication at mmWave Communication Mode

Based on (6), the successful transmission probability of the typical D2D users at the mmWave communication mode can

$$\begin{aligned}&\mathbb{E}_{I^{\mathrm{D},\mathrm{m}}_{d_0^{\mathrm{Rx}}}}\left[\exp\left(-\upsilon\iota I^{\mathrm{D},\mathrm{m}}_{d_0^{\mathrm{Rx}}}\right)\right]=\mathbb{E}_{\Phi_{\left\{\mathcal{D}^{\mathrm{Tx}}\setminus\left\{d_0^{\mathrm{Tx}}\right\}|d_0^{\mathrm{Rx}}\right\}}}\left[\prod_{d^{\mathrm{Tx}}\in\left\{\mathcal{D}^{\mathrm{Tx}}\setminus\left\{d_0^{\mathrm{Tx}}\right\}|d_0^{\mathrm{Rx}}\right\}}\left\{1-\mathbb{P}^{\mathcal{D}_1}\mathbb{P}^{\mathcal{M}^{\mathrm{m}}}+\mathbb{P}^{\mathcal{D}_1}\mathbb{P}^{\mathcal{M}^{\mathrm{m}}}\right.\right.\\&\left.\left.\times\,\mathbb{E}_{g^{\mathrm{m}}_{d^{\mathrm{Tx}}d_0^{\mathrm{Rx}}}}\left[\mathbb{E}_{h^{\mathrm{m}}_{d^{\mathrm{Tx}}d_0^{\mathrm{Rx}}}}\left[\exp\left(-\upsilon\iota p^{\mathrm{D}}h^{\mathrm{m}}_{d^{\mathrm{Tx}}d_0^{\mathrm{Rx}}}g^{\mathrm{m}}_{d^{\mathrm{Tx}}d_0^{\mathrm{Rx}}}\ell^{\mathrm{m}}\left(\mathbf{x}_{d^{\mathrm{Tx}}},\mathbf{x}_{d_0^{\mathrm{Rx}}}\right)\right)\right]\right]\right\}\right]\\&\overset{(20)}{=}\mathbb{E}_{\Phi_{\left\{\mathcal{D}^{\mathrm{Tx}}\setminus\left\{d_0^{\mathrm{Tx}}\right\}|d_0^{\mathrm{Rx}}\right\}}}\left[\prod_{d^{\mathrm{Tx}}\in\left\{\mathcal{D}^{\mathrm{Tx}}\setminus\left\{d_0^{\mathrm{Tx}}\right\}|d_0^{\mathrm{Rx}}\right\}}\left[1-\mathbb{P}^{\mathcal{D}_1}\mathbb{P}^{\mathcal{M}^{\mathrm{m}}}+\mathbb{P}^{\mathcal{D}_1}\mathbb{P}^{\mathcal{M}^{\mathrm{m}}}\sum_{\substack{\mathrm{g}\in\mathcal{G}\\\mathrm{s}\in\mathcal{S}}}\frac{\mathbb{P}^{g^{\mathrm{g}}_{\mathcal{D}^{\mathrm{Tx}}\mathcal{D}^{\mathrm{Rx}}}}P^{\mathrm{s}}\left(r_{d^{\mathrm{Tx}}d_0^{\mathrm{Rx}}}\right)}{\left(\frac{\upsilon\iota p^{\mathrm{D}}g^{\mathrm{g}}_{\mathcal{D}^{\mathrm{Tx}}\mathcal{D}^{\mathrm{Rx}}}r^{-\alpha^{\mathrm{m},\mathrm{s}}}_{d^{\mathrm{Tx}}d_0^{\mathrm{Rx}}}}{\upsilon^{\mathrm{s}}}+1\right)^{\upsilon^{\mathrm{s}}}}\right]\right]\\&=\exp\left(-2\pi\lambda_{\mathcal{D}^{\mathrm{Tx}}}\mathbb{P}^{\mathcal{D}_1}\mathbb{P}^{\mathcal{M}^{\mathrm{m}}}\sum_{\substack{\mathrm{g}\in\mathcal{G}\\\mathrm{s}\in\mathcal{S}}}\mathbb{P}^{g^{\mathrm{g}}_{\mathcal{D}^{\mathrm{Tx}}\mathcal{D}^{\mathrm{Rx}}}}\int_0^{+\infty}P^{\mathrm{s}}\left(r\right)\left[1-\frac{1}{\left(\frac{\upsilon\iota p^{\mathrm{D}}g^{\mathrm{g}}_{\mathcal{D}^{\mathrm{Tx}}\mathcal{D}^{\mathrm{Rx}}}r^{-\alpha^{\mathrm{m},\mathrm{s}}}}{\upsilon^{\mathrm{s}}}+1\right)^{\upsilon^{\mathrm{s}}}}\right]r\mathrm{d}r\right).\end{aligned}\tag{25}$$

$$\begin{aligned}&\mathbb{E}_{I^{\mathrm{C},\mathrm{M}}_{d_0^{\mathrm{Rx}}}}\left[\exp\left(-\frac{\eta^{\mathrm{M}}r_0^{\alpha^{\mathrm{M}}}}{p^{\mathrm{D}}}I^{\mathrm{C},\mathrm{M}}_{d_0^{\mathrm{Rx}}}\right)\right]=\mathbb{E}_{\Phi_{\left\{\mathcal{B}^{\mathrm{M}}|d_0^{\mathrm{Rx}}\right\}}}\left[\prod_{b^{\mathrm{M}}\in\left\{\mathcal{B}^{\mathrm{M}}|d_0^{\mathrm{Rx}}\right\}}\left(\frac{\mathbb{P}^{\mathcal{C}_1^{\mathrm{M}}}}{1+\frac{\eta^{\mathrm{M}}r_0^{\alpha^{\mathrm{M}}}}{p^{\mathrm{D}}}p^{\mathrm{M}}\ell^{\mathrm{M}}\left(\mathbf{x}_{b^{\mathrm{M}}},\mathbf{x}_{d_0^{\mathrm{Rx}}}\right)}+\mathbb{P}^{\mathcal{C}_0^{\mathrm{M}}}\right)\right]\\&=\exp\left(-2\pi\lambda_{\mathcal{B}^{\mathrm{M}}}\int_0^{\infty}\left[1-\left(\frac{\mathbb{P}^{\mathcal{C}_1^{\mathrm{M}}}}{1+\frac{\eta^{\mathrm{M}}r_0^{\alpha^{\mathrm{M}}}}{p^{\mathrm{D}}}p^{\mathrm{M}}r^{-\alpha^{\mathrm{M}}}_{b^{\mathrm{M}}d_0^{\mathrm{Rx}}}}+\mathbb{P}^{\mathcal{C}_0^{\mathrm{M}}}\right)\right]r_{b^{\mathrm{M}}d_0^{\mathrm{Rx}}}\mathrm{d}r_{b^{\mathrm{M}}d_0^{\mathrm{Rx}}}\right)\overset{[18]}{=}\exp\left(-\frac{\pi\lambda_{\mathcal{B}^{\mathrm{M}}}\mathbb{P}^{\mathcal{C}_1^{\mathrm{M}}}r_0^2\left(\frac{\eta^{\mathrm{M}}}{p^{\mathrm{D}}}p^{\mathrm{M}}\right)^{\frac{2}{\alpha^{\mathrm{M}}}}}{\mathrm{sinc}\left(\frac{2}{\alpha^{\mathrm{M}}}\right)}\right).\end{aligned}\tag{26}$$

$$\begin{aligned}&\mathbb{E}_{I^{\mathrm{C}}_{a_0^{\mathrm{m}}}+I^{\mathrm{D}}_{a_0^{\mathrm{m}}}}\left[\exp\left(-n\iota\frac{I^{\mathrm{C}}_{a_0^{\mathrm{m}}}+I^{\mathrm{D}}_{a_0^{\mathrm{m}}}}{\tau^{\mathrm{m}}-N_{a_0^{\mathrm{m}}}}\right)\right]\\&\overset{(21)-(25)}{=}\exp\left(-2\pi\lambda_{\mathcal{B}^{\mathrm{m}}}\mathbb{P}^{\mathcal{C}_1^{\mathrm{m}}}\sum_{\substack{\mathrm{g}\in\mathcal{G}\\\mathrm{s}\in\mathcal{S}}}\mathbb{P}^{g^{\mathrm{g}}_{\mathcal{B}^{\mathrm{m}}\mathcal{A}^{\mathrm{m}}}}\int_0^{+\infty}P^{\mathrm{s}}\left(r\right)\left[1-\frac{1}{\left(\frac{n\iota p^{\mathrm{m}}g^{\mathrm{g}}_{\mathcal{B}^{\mathrm{m}}\mathcal{A}^{\mathrm{m}}}r^{-\alpha^{\mathrm{m},\mathrm{s}}}}{\left(\tau^{\mathrm{m}}-N_{a_0^{\mathrm{m}}}\right)\upsilon^{\mathrm{s}}}+1\right)^{\upsilon^{\mathrm{s}}}}\right]r\mathrm{d}r\right)\\&\times\exp\left(-2\pi\lambda_{\mathcal{D}^{\mathrm{Tx}}}\mathbb{P}^{\mathcal{D}_1}\mathbb{P}^{\mathcal{M}^{\mathrm{m}}}\sum_{\substack{\mathrm{g}\in\mathcal{G}\\\mathrm{s}\in\mathcal{S}}}\mathbb{P}^{g^{\mathrm{g}}_{\mathcal{D}^{\mathrm{Tx}}\mathcal{A}^{\mathrm{m}}}}\int_0^{+\infty}P^{\mathrm{s}}\left(r\right)\left[1-\frac{1}{\left(\frac{n\iota p^{\mathrm{D}}g^{\mathrm{g}}_{\mathcal{D}^{\mathrm{Tx}}\mathcal{A}^{\mathrm{m}}}r^{-\alpha^{\mathrm{m},\mathrm{s}}}}{\left(\tau^{\mathrm{m}}-N_{a_0^{\mathrm{m}}}\right)\upsilon^{\mathrm{s}}}+1\right)^{\upsilon^{\mathrm{s}}}}\right]r\mathrm{d}r\right).\end{aligned}\tag{27}$$

be derived in (18), shown at the bottom of the previous page, and the last of which is derived in (19), shown at the bottom of the previous page, with (a) being a tight lower-bound and following Lemma 1 in [31], (b) following the independence between $I_{d_0^{\mathrm{Rx}}}^{\mathrm{C,m}}$ and $I_{d_0^{\mathrm{Rx}}}^{\mathrm{D,m}}$, and $\iota = \upsilon^{\mathrm{s}}(\upsilon^{\mathrm{s}}!)^{-\frac{1}{\upsilon^{\mathrm{s}}}} \frac{\eta^{\mathrm{m}} r_0^{\alpha^{\mathrm{m,s}}}}{p^{\mathrm{D}} g^{\mathrm{g}}_{\mathcal{D}^{\mathrm{Tx}}\mathcal{D}^{\mathrm{Rx}}}}$. Therein, as we can have in (20), shown at the bottom of page 12, we can further have in (21), shown at the bottom of page 12, where (a) follows the probability generating functionals of Poisson Point Process (PPP) [7]. Similarly, we can have in (25), shown at the bottom of the previous page.

Appendix C
SINR Distribution of D2D Communication at Microwave Communication Mode

Based on (7), the successful transmission probability of the typical D2D users at the microwave communication mode is shown in (23), shown at the bottom of page 12, where (a) follows the independence between $I_{d_0^{\mathrm{Rx}}}^{\mathrm{C,M}}$ and $I_{d_0^{\mathrm{Rx}}}^{\mathrm{D,M}}$. Therein, we can have in (26), shown at the bottom of the previous page. Moreover, similar to (26), we can have $\mathbb{E}_{I_{d_0^{\mathrm{Rx}}}^{\mathrm{D,M}}}\left[\exp\left(-\frac{\eta^{\mathrm{M}} r_0^{\alpha^{\mathrm{M}}}}{p^{\mathrm{D}}} I_{d_0^{\mathrm{Rx}}}^{\mathrm{D,M}}\right)\right] = \exp\left(-\frac{\pi\lambda_{\mathcal{D}^{\mathrm{Tx}}}\mathbb{P}^{\mathcal{D}_1}\mathbb{P}^{\mathcal{M}^{\mathrm{M}}} r_0^2\left(\eta^{\mathrm{M}}\right)^{\frac{2}{\alpha^{\mathrm{M}}}}}{\mathrm{sinc}\left(\frac{2}{\alpha^{\mathrm{M}}}\right)}\right)$.

Appendix D
FA Probability of MmWave Adversary a_0^{m}

The FA probability of mmWave adversary a_0^{m} defined in (8) is derived in (22), shown at the bottom of page 12, where an auxiliary random variable $\xi \sim \mathrm{Gamma}\left(N, \frac{1}{N}\right)$ has been introduced in (a) and converges to 1 as $N \to \infty$, (b) follows the approximation method introduced in Theorem 1 of [32], $\iota = N(N!)^{-\frac{1}{N}}$, and $\mathbb{E}_{I_{a_0^{\mathrm{m}}}^{\mathrm{C}}+I_{a_0^{\mathrm{m}}}^{\mathrm{D}}}\left[\exp\left(-n\iota\frac{I_{a_0^{\mathrm{m}}}^{\mathrm{C}}+I_{a_0^{\mathrm{m}}}^{\mathrm{D}}}{\tau^{\mathrm{m}}-N_{a_0^{\mathrm{m}}}}\right)\right]$ is derived in (27), shown at the bottom of the previous page.

Appendix E
MD Probability of MmWave Adversary a_0^{m}

The MD probability of mmWave adversary a_0^{m} defined in (9) is derived in (28), shown at the bottom of the page, where $F_{I_{a_0^{\mathrm{m}}}^{\mathrm{C}}+I_{a_0^{\mathrm{m}}}^{\mathrm{D}}}(\cdot)$ has been given in (22) and $f_{p^{\mathrm{D}}h^{\mathrm{m}}_{d_0^{\mathrm{Tx}}a_0^{\mathrm{m}}}g^{\mathrm{m}}_{d_0^{\mathrm{Tx}}a_0^{\mathrm{m}}}\ell^{\mathrm{m}}\left(\mathbf{x}_{d_0^{\mathrm{Tx}}},\mathbf{x}_{a_0^{\mathrm{m}}}\right)}(\cdot)$ is given in (29), shown at the bottom of the page, with $f_{r_{d_0^{\mathrm{Tx}}a_0^{\mathrm{m}}}}(r) = 2\pi\lambda_{\mathcal{A}^{\mathrm{m}}} r \exp\left(-\pi\lambda_{\mathcal{A}^{\mathrm{m}}} r^2\right)$ following the fact that no mmWave adversary is geographically nearer to D2D transmitter d_0^{Tx} than mmWave adversary a_0^{m} [33].

Appendix F
FA Probability of Microwave Adversary a_0^{M}

Based on (10), the FA probability of microwave adversary a_0^{M} can be derived as

$$\begin{aligned}\mathbb{P}^{\mathrm{FA}}_{a_0^{\mathrm{M}}}\left(p^{\mathrm{D}}, p^{\mathcal{M}^{\mathrm{f}}}, \tau^{\mathrm{M}}\right) &= \mathbb{P}\left[y_{a_0^{\mathrm{M}}} > \tau^{\mathrm{M}} \middle| \mathcal{D}_0 \cup (\mathcal{D}_1 \cap \mathcal{M}^{\mathrm{m}})\right] \\ &= \mathbb{P}\left[I_{a_0^{\mathrm{M}}}^{\mathrm{C}} + I_{a_0^{\mathrm{M}}}^{\mathrm{D}} + N_{a_0^{\mathrm{M}}} > \tau^{\mathrm{M}}\right] \\ &= 1 - F_{I_{a_0^{\mathrm{m}}}^{\mathrm{C}}+I_{a_0^{\mathrm{m}}}^{\mathrm{D}}}\left(\tau^{\mathrm{M}} - N_{a_0^{\mathrm{M}}}\right), \quad (30)\end{aligned}$$

where $F_{I_{a_0^{\mathrm{M}}}^{\mathrm{C}}+I_{a_0^{\mathrm{M}}}^{\mathrm{D}}}(\cdot)$ can be obtained as follows [7]:

1) Laplace transform of $I_{a_0^{\mathrm{M}}}^{\mathrm{C}} + I_{a_0^{\mathrm{M}}}^{\mathrm{D}}$: $\mathcal{L}_{I_{a_0^{\mathrm{M}}}^{\mathrm{C}}+I_{a_0^{\mathrm{M}}}^{\mathrm{D}}}(\iota) = \exp\left(-\frac{\pi\iota^{\frac{2}{\alpha^{\mathrm{M}}}}\kappa_{I_{a_0^{\mathrm{M}}}^{\mathrm{C}}+I_{a_0^{\mathrm{M}}}^{\mathrm{D}}}}{\mathrm{sinc}\left(\frac{2}{\alpha^{\mathrm{M}}}\right)}\right)$,

$$\mathbb{P}^{\mathrm{MD}}_{a_0^{\mathrm{m}}}\left(p^{\mathrm{D}}, p^{\mathcal{M}^{\mathrm{f}}}, \tau^{\mathrm{m}}\right) = \mathbb{P}\left[y_{a_0^{\mathrm{m}}} < \tau^{\mathrm{m}} \middle| \mathcal{D}_1 \cap \mathcal{M}^{\mathrm{m}}\right] = \mathbb{P}\left[p^{\mathrm{D}}h^{\mathrm{m}}_{d_0^{\mathrm{Tx}}a_0^{\mathrm{m}}}g^{\mathrm{m}}_{d_0^{\mathrm{Tx}}a_0^{\mathrm{m}}}\ell^{\mathrm{m}}\left(\mathbf{x}_{d_0^{\mathrm{Tx}}},\mathbf{x}_{a_0^{\mathrm{m}}}\right) + I_{a_0^{\mathrm{m}}}^{\mathrm{C}} + I_{a_0^{\mathrm{m}}}^{\mathrm{D}} + N_{a_0^{\mathrm{m}}} < \tau^{\mathrm{m}}\right]$$
$$= \int_0^{\tau^{\mathrm{m}}-N_{a_0^{\mathrm{m}}}} f_{p^{\mathrm{D}}h^{\mathrm{m}}_{d_0^{\mathrm{Tx}}a_0^{\mathrm{m}}}g^{\mathrm{m}}_{d_0^{\mathrm{Tx}}a_0^{\mathrm{m}}}\ell^{\mathrm{m}}\left(\mathbf{x}_{d_0^{\mathrm{Tx}}},\mathbf{x}_{a_0^{\mathrm{m}}}\right)}(t)\, F_{I_{a_0^{\mathrm{m}}}^{\mathrm{C}}+I_{a_0^{\mathrm{m}}}^{\mathrm{D}}}\left(\tau^{\mathrm{m}} - N_{a_0^{\mathrm{m}}} - t\right) \mathrm{d}t. \quad (28)$$

$$f_{p^{\mathrm{D}}h^{\mathrm{m}}_{d_0^{\mathrm{Tx}}a_0^{\mathrm{m}}}g^{\mathrm{m}}_{d_0^{\mathrm{Tx}}a_0^{\mathrm{m}}}\ell^{\mathrm{m}}\left(\mathbf{x}_{d_0^{\mathrm{Tx}}},\mathbf{x}_{a_0^{\mathrm{m}}}\right)}(t) = \frac{\partial}{\partial t}F_{p^{\mathrm{D}}h^{\mathrm{m}}_{d_0^{\mathrm{Tx}}a_0^{\mathrm{m}}}g^{\mathrm{m}}_{d_0^{\mathrm{Tx}}a_0^{\mathrm{m}}}\ell^{\mathrm{m}}\left(\mathbf{x}_{d_0^{\mathrm{Tx}}},\mathbf{x}_{a_0^{\mathrm{m}}}\right)}(t)$$
$$= \frac{\partial}{\partial t}\mathbb{P}\left[p^{\mathrm{D}}h^{\mathrm{m}}_{d_0^{\mathrm{Tx}}a_0^{\mathrm{m}}}g^{\mathrm{m}}_{d_0^{\mathrm{Tx}}a_0^{\mathrm{m}}}\ell^{\mathrm{m}}\left(\mathbf{x}_{d_0^{\mathrm{Tx}}},\mathbf{x}_{a_0^{\mathrm{m}}}\right) \le t\right] = \frac{\partial}{\partial t}\sum_{\substack{\mathrm{g}\in\mathcal{G}\\ \mathrm{s}\in\mathcal{S}}} \mathbb{P}^{g^{\mathrm{g}}_{\mathcal{D}^{\mathrm{Tx}}\mathcal{A}^{\mathrm{m}}}}\mathbb{E}_{r_{d_0^{\mathrm{Tx}}a_0^{\mathrm{m}}}}\left[P^{\mathrm{s}}\left(r_{d_0^{\mathrm{Tx}}a_0^{\mathrm{m}}}\right)\mathbb{P}\left[h^{\mathrm{m}}_{d_0^{\mathrm{Tx}}a_0^{\mathrm{m}}} \le \frac{tr^{\alpha^{\mathrm{m,s}}}_{d_0^{\mathrm{Tx}}a_0^{\mathrm{m}}}}{p^{\mathrm{D}}g^{\mathrm{g}}_{\mathcal{D}^{\mathrm{Tx}}\mathcal{A}^{\mathrm{m}}}} \middle| \mathrm{s}\right]\right]$$
$$= \frac{\partial}{\partial t}\sum_{\substack{\mathrm{g}\in\mathcal{G}\\ \mathrm{s}\in\mathcal{S}}} \mathbb{P}^{g^{\mathrm{g}}_{\mathcal{D}^{\mathrm{Tx}}\mathcal{A}^{\mathrm{m}}}}\mathbb{E}_{r_{d_0^{\mathrm{Tx}}a_0^{\mathrm{m}}}}\left[P^{\mathrm{s}}\left(r_{d_0^{\mathrm{Tx}}a_0^{\mathrm{m}}}\right)\frac{\gamma\left(\upsilon^{\mathrm{s}}, \upsilon^{\mathrm{s}}\frac{tr^{\alpha^{\mathrm{m,s}}}_{d_0^{\mathrm{Tx}}a_0^{\mathrm{m}}}}{p^{\mathrm{D}}g^{\mathrm{g}}_{\mathcal{D}^{\mathrm{Tx}}\mathcal{A}^{\mathrm{m}}}}\right)}{\Gamma\left(\upsilon^{\mathrm{s}}\right)}\right]$$
$$= \sum_{\substack{\mathrm{g}\in\mathcal{G}\\ \mathrm{s}\in\mathcal{S}}} \mathbb{P}^{g^{\mathrm{g}}_{\mathcal{D}^{\mathrm{Tx}}\mathcal{A}^{\mathrm{m}}}}\frac{t^{\upsilon^{\mathrm{s}}-1}}{\Gamma\left(\upsilon^{\mathrm{s}}\right)}\int_0^{+\infty} f_{r_{d_0^{\mathrm{Tx}}a_0^{\mathrm{m}}}}(r)\, P^{\mathrm{s}}(r)\left(\frac{\upsilon^{\mathrm{s}}r^{\alpha^{\mathrm{m,s}}}}{p^{\mathrm{D}}g^{\mathrm{g}}_{\mathcal{D}^{\mathrm{Tx}}\mathcal{A}^{\mathrm{m}}}}\right)^{\upsilon^{\mathrm{s}}}\exp\left(-\frac{\upsilon^{\mathrm{s}}tr^{\alpha^{\mathrm{m,s}}}}{p^{\mathrm{D}}g^{\mathrm{g}}_{\mathcal{D}^{\mathrm{Tx}}\mathcal{A}^{\mathrm{m}}}}\right)\mathrm{d}r. \quad (29)$$

2) Inverse Laplace transform of $\mathcal{L}_{I^{\mathrm{C}}_{a^{\mathrm{M}}_0}+I^{\mathrm{D}}_{a^{\mathrm{M}}_0}}(\iota)$ according to Bromwich inversion theorem in Chapter 2 of [34]:

$$\begin{aligned} F_{I^{\mathrm{C}}_{a^{\mathrm{M}}_0}+I^{\mathrm{D}}_{a^{\mathrm{M}}_0}}(t) &= \mathcal{L}^{-1}_{\mathcal{L}_{I^{\mathrm{C}}_{a^{\mathrm{M}}_0}+I^{\mathrm{D}}_{a^{\mathrm{M}}_0}}(\iota)}(t) \\ &= 1-\int_0^{+\infty} \exp\left(-tu-\kappa_{I^{\mathrm{C}}_{a^{\mathrm{M}}_0}+I^{\mathrm{D}}_{a^{\mathrm{M}}_0}} u^{\frac{2}{\alpha^{\mathrm{M}}}}\cos\left(\frac{2\pi}{\alpha^{\mathrm{M}}}\right)\right) \\ &\quad \times \sin\left(\kappa_{I^{\mathrm{C}}_{a^{\mathrm{M}}_0}+I^{\mathrm{D}}_{a^{\mathrm{M}}_0}} u^{\frac{2}{\alpha^{\mathrm{M}}}}\sin\left(\frac{2\pi}{\alpha^{\mathrm{M}}}\right)\right)\frac{\mathrm{d}u}{\pi u}, \end{aligned} \tag{31}$$

where $\kappa_{I^{\mathrm{C}}_{a^{\mathrm{M}}_0}+I^{\mathrm{D}}_{a^{\mathrm{M}}_0}} = \frac{\pi}{\mathrm{sinc}\left(\frac{2}{\alpha^{\mathrm{M}}}\right)}\left[\lambda_{\mathcal{B}^{\mathrm{M}}}\mathbb{P}^{\mathcal{C}^{\mathrm{M}}_1}\left(p^{\mathrm{M}}\right)^{\frac{2}{\alpha^{\mathrm{M}}}} + \lambda_{\mathcal{D}^{\mathrm{Tx}}}\mathbb{P}^{\mathcal{D}_1}\mathbb{P}^{\mathcal{M}^{\mathrm{M}}}\left(p^{\mathrm{D}}\right)^{\frac{2}{\alpha^{\mathrm{M}}}}\right]$.

Appendix G
MD Probability of Microwave Adversary a^{M}_0

The MD probability of microwave adversary a^{M}_0 defined in (11) is

$$\begin{aligned} &\mathbb{P}^{\mathrm{MD}}_{a^{\mathrm{M}}_0}\left(p^{\mathrm{D}}, p^{\mathcal{M}^{\mathrm{f}}}, \tau^{\mathrm{M}}\right) \\ &= \mathbb{P}\left[y_{a^{\mathrm{M}}_0} < \tau^{\mathrm{M}} \middle| \mathcal{D}_1 \cap \mathcal{M}^{\mathrm{M}}\right] \\ &= \mathbb{P}\left[p^{\mathrm{D}} h^{\mathrm{M}}_{d^{\mathrm{Tx}}_0 a^{\mathrm{M}}_0} \ell^{\mathrm{M}}\left(\mathbf{x}_{d^{\mathrm{Tx}}_0}, \mathbf{x}_{a^{\mathrm{M}}_0}\right) + I^{\mathrm{C}}_{a^{\mathrm{M}}_0} + I^{\mathrm{D}}_{a^{\mathrm{M}}_0} + N_{a^{\mathrm{M}}_0} < \tau^{\mathrm{M}}\right] \\ &= \int_0^{\tau^{\mathrm{M}}-N_{a^{\mathrm{M}}_0}} f_{p^{\mathrm{D}} h^{\mathrm{M}}_{d^{\mathrm{Tx}}_0 a^{\mathrm{M}}_0} \ell^{\mathrm{M}}\left(\mathbf{x}_{d^{\mathrm{Tx}}_0}, \mathbf{x}_{a^{\mathrm{M}}_0}\right)}(t) \\ &\quad \times F_{I^{\mathrm{C}}_{a^{\mathrm{M}}_0}+I^{\mathrm{D}}_{a^{\mathrm{M}}_0}}\left(\tau^{\mathrm{M}} - N_{a^{\mathrm{M}}_0} - t\right)\mathrm{d}t, \end{aligned} \tag{32}$$

where $F_{I^{\mathrm{C}}_{a^{\mathrm{M}}_0}+I^{\mathrm{D}}_{a^{\mathrm{M}}_0}}(\cdot)$ has been given in (31) and

$$\begin{aligned} &f_{p^{\mathrm{D}} h^{\mathrm{M}}_{d^{\mathrm{Tx}}_0 a^{\mathrm{M}}_0} \ell^{\mathrm{M}}\left(\mathbf{x}_{d^{\mathrm{Tx}}_0}, \mathbf{x}_{a^{\mathrm{M}}_0}\right)}(t) \\ &= \frac{\partial}{\partial t}\mathbb{P}\left[h^{\mathrm{M}}_{d^{\mathrm{Tx}}_0 a^{\mathrm{M}}_0} \le \frac{r^{\alpha^{\mathrm{M}}}_{d^{\mathrm{Tx}}_0 a^{\mathrm{M}}_0}}{p^{\mathrm{D}}} t\right] \\ &= \int_0^{+\infty} f_{r_{d^{\mathrm{Tx}}_0 a^{\mathrm{M}}_0}}(r)\frac{r^{\alpha^{\mathrm{M}}}}{p^{\mathrm{D}}}\exp\left(-\frac{r^{\alpha^{\mathrm{M}}}}{p^{\mathrm{D}}}t\right)\mathrm{d}r \end{aligned} \tag{33}$$

with $f_{r_{d^{\mathrm{Tx}}_0 a^{\mathrm{M}}_0}}(r) = 2\pi\lambda_{\mathcal{A}^{\mathrm{M}}} r \exp\left(-\pi\lambda_{\mathcal{A}^{\mathrm{M}}} r^2\right)$ following the fact that no microwave adversary is geographically nearer to D2D transmitter d^{Tx}_0 than microwave adversary a^{M}_0 [33].

References

[1] F. Wang, H. Wang, H. Feng, and X. Xu, "A hybrid communication model of millimeter wave and microwave in D2D network," in *Proc. IEEE 83rd Veh. Technol. Conf. (VTC Spring)*, May 2016, pp. 1–5.

[2] S. Feng, D. Niyato, X. Lu, P. Wang, and D. I. Kim, "Dynamic model for network selection in next generation HetNets with memory-affecting rational users," *IEEE Trans. Mobile Comput.*, vol. 20, no. 4, pp. 1365–1379, Apr. 2021.

[3] S. Zhang, J. Liu, H. Guo, M. Qi, and N. Kato, "Envisioning device-to-device communications in 6G," *IEEE Netw.*, vol. 34, no. 3, pp. 86–91, May/Jun. 2020.

[4] S. Feng, X. Lu, K. Zhu, D. Niyato, and P. Wang, "Covert D2D communication underlaying cellular network: A system-level security perspective," 2023, *arXiv:2302.01745*.

[5] J. Dai, J. Liu, Y. Shi, S. Zhang, and J. Ma, "Analytical modeling of resource allocation in D2D overlaying multihop multichannel uplink cellular networks," *IEEE Trans. Veh. Technol.*, vol. 66, no. 8, pp. 6633–6644, Aug. 2017.

[6] X. Lu, E. Hossain, T. Shafique, S. Feng, H. Jiang, and D. Niyato, "Intelligent reflecting surface enabled covert communications in wireless networks," *IEEE Netw.*, vol. 34, no. 5, pp. 148–155, Sep./Oct. 2020.

[7] S. Feng, X. Lu, S. Sun, and D. Niyato, "Mean-field artificial noise assistance and uplink power control in covert IoT systems," *IEEE Trans. Wireless Commun.*, vol. 21, no. 9, pp. 7358–7373, Sep. 2022.

[8] N. Deng, M. Haenggi, and Y. Sun, "Millimeter-wave device-to-device networks with heterogeneous antenna arrays," *IEEE Trans. Commun.*, vol. 66, no. 9, pp. 4271–4285, Sep. 2018.

[9] T. Bai and R. W. Heath, "Coverage and rate analysis for millimeter-wave cellular networks," *IEEE Trans. Wireless Commun.*, vol. 14, no. 2, pp. 1100–1114, Feb. 2015.

[10] Y. Zhang, Y. Shen, X. Jiang, and S. Kasahara, "Secure millimeter-wave ad hoc communications using physical layer security," *IEEE Trans. Inf. Forensics Security*, vol. 17, pp. 99–114, 2022.

[11] S. Feng, X. Lu, D. Niyato, E. Hossain, and S. Sun, "Achieving covert communication in large-scale SWIPT-enabled D2D networks," 2023, *arXiv:2302.08010*.

[12] P. Cheng, L. Deng, H. Yu, Y. Xu, and H. Wang, "Resource allocation for cognitive networks with D2D communication: An evolutionary approach," in *Proc. IEEE Wireless Commun. Netw. Conf. (WCNC)*, Apr. 2012, pp. 2671–2676.

[13] H. H. Yang, J. Lee, and T. Q. S. Quek, "Heterogeneous cellular network with energy harvesting-based D2D communication," *IEEE Trans. Wireless Commun.*, vol. 15, no. 2, pp. 1406–1419, Feb. 2016.

[14] S. Xiang, Q. Quan, T. Peng, and W. Wang, "Performance analysis of cooperative mode selection in hybrid D2D and IMT-advanced network," in *Proc. 7th Int. Conf. Commun. Netw. China*, Aug. 2012, pp. 717–721.

[15] N. Yang, L. Wang, G. Geraci, M. Elkashlan, J. Yuan, and M. Di Renzo, "Safeguarding 5G wireless communication networks using physical layer security," *IEEE Commun. Mag.*, vol. 53, no. 4, pp. 20–27, Apr. 2015.

[16] Y. Wu et al., "A survey of physical layer security techniques for 5G wireless networks and challenges ahead," *IEEE J. Sel. Areas Commun.*, vol. 36, no. 4, pp. 679–695, Apr. 2018.

[17] N. T. T. Van, N. C. Luong, H. T. Nguyen, F. Shaohan, D. Niyato, and D. I. Kim, "Latency minimization in covert communication-enabled federated learning network," *IEEE Trans. Veh. Technol.*, vol. 70, no. 12, pp. 13447–13452, Dec. 2021.

[18] S. Feng, X. Lu, S. Sun, D. Niyato, and E. Hossain, "Securing large-scale D2D networks using covert communication and friendly jamming," 2022, *arXiv:2209.15170*.

[19] J. Zhang et al., "Joint beam training and data transmission design for covert millimeter-wave communication," *IEEE Trans. Inf. Forensics Security*, vol. 16, pp. 2232–2245, 2021.

[20] C. Wang, Z. Li, and D. W. K. Ng, "Covert rate optimization of millimeter wave full-duplex communications," *IEEE Trans. Wireless Commun.*, vol. 21, no. 5, pp. 2844–2861, May 2022.

[21] M. Salehi, A. Mohammadi, and M. Haenggi, "Analysis of D2D underlaid cellular networks: SIR meta distribution and mean local delay," *IEEE Trans. Commun.*, vol. 65, no. 7, pp. 2904–2916, Jul. 2017.

[22] W. Lu and M. D. Renzo, "Stochastic geometry modeling of cellular networks: Analysis, simulation and experimental validation," in *Proc. ACM Int. Conf. Model. Anal. Simulat. Wireless Mobile Syst.* New York, NY, USA: Association for Computing Machinery, Nov. 2015, pp. 179–188, doi: 10.1145/2811587.2811597.

[23] H. ElSawy and E. Hossain, "On stochastic geometry modeling of cellular uplink transmission with truncated channel inversion power control," *IEEE Trans. Wireless Commun.*, vol. 13, no. 8, pp. 4454–4469, Aug. 2014.

[24] J. Liu, H. Nishiyama, N. Kato, and J. Guo, "On the outage probability of device-to-device-communication-enabled multichannel cellular networks: An RSS-threshold-based perspective," *IEEE J. Sel. Areas Commun.*, vol. 34, no. 1, pp. 163–175, Jan. 2016.

[25] B. A. Bash, D. Goeckel, and D. Towsley, "Covert communication gains from adversary's ignorance of transmission time," *IEEE Trans. Wireless Commun.*, vol. 15, no. 12, pp. 8394–8405, Dec. 2016.

[26] B. A. Bash, D. Goeckel, and D. Towsley, "Limits of reliable communication with low probability of detection on AWGN channels," *IEEE J. Sel. Areas Commun.*, vol. 31, no. 9, pp. 1921–1930, Sep. 2013.

[27] B. A. Bash, D. Goeckel, and D. Towsley, "Square root law for communication with low probability of detection on AWGN channels," in *Proc. IEEE Int. Symp. Inf. Theory*, Jul. 2012, pp. 448–452.
[28] S. A. Mousavifar and C. Leung, "Trust-based energy efficient spectrum sensing in cognitive radio networks," in *Proc. IEEE 78th Veh. Technol. Conf. (VTC Fall)*, Sep. 2013, pp. 1–6.
[29] J. Kiefer, "Sequential minimax search for a maximum," *Proc. Amer. Math. Soc.*, vol. 4, no. 3, pp. 502–506, 1953. [Online]. Available: http://www.jstor.org/stable/2032161
[30] G. Scutari, F. Facchinei, P. Song, D. P. Palomar, and J. Pang, "Decomposition by partial linearization: Parallel optimization of multi-agent systems," *IEEE Trans. Signal Process.*, vol. 62, no. 3, pp. 641–656, Feb. 2014.
[31] A. Thornburg, T. Bai, and R. W. Heath, "Performance analysis of outdoor mmWave ad hoc networks," *IEEE Trans. Signal Process.*, vol. 64, no. 15, pp. 4065–4079, Aug. 2016.
[32] T. A. Khan, A. Alkhateeb, and R. W. Heath, "Millimeter wave energy harvesting," *IEEE Trans. Wireless Commun.*, vol. 15, no. 9, pp. 6048–6062, Sep. 2016.
[33] J. G. Andrews et al., "A tractable approach to coverage and rate in cellular networks," *IEEE Trans. Commun.*, vol. 59, no. 11, pp. 3122–3134, Nov. 2011.
[34] A. M. Cohen, *Numerical Methods for Laplace Transform Inversion*, 1st ed., Berlin, Germany: Springer, 2007.

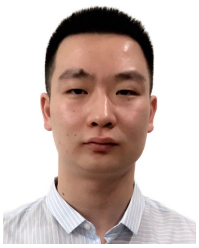

Shaohan Feng (Member, IEEE) received the B.S. degree from the School of Mathematics and Systems Science, Beihang University, Beijing, China, in 2014, the M.S. degree from the School of Mathematical Sciences, Zhejiang University, Hangzhou, China, in 2016, and the Ph.D. degree from the School of Computer Science and Engineering, Nanyang Technological University, Singapore, in 2020. His current research interests include resource management and risk management in computer networks and wireless communications.

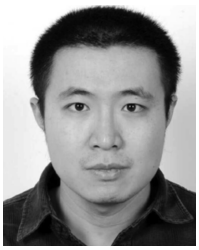

Xiao Lu (Member, IEEE) received the B.Eng. degree in communication engineering from the Beijing University of Posts and Telecommunications, Beijing, China, the M.Eng. degree in computer engineering from Nanyang Technological University, Singapore, and the Ph.D. degree from the University of Alberta, Edmonton, AB, Canada. He is currently with Ericsson, Canada, and York University, Canada. His current research interests include the design, analysis, and optimization of future-generation cellular wireless networks. He was a recipient of the Best Paper Award from the IEEE Communication Society: Green Communications and Computing Technical Committee in 2018 and the IEEE TCGCC Best Conference Paper Award.

Dusit Niyato (Fellow, IEEE) received the B.Eng. degree from King Mongkut's Institute of Technology Ladkrabang (KMITL), Bangkok, Thailand, and the Ph.D. degree in electrical and computer engineering from the University of Manitoba, Winnipeg, MB, Canada. He is currently a Professor with the College of Computing and Data Science, Nanyang Technological University, Singapore. His research interests include mobile generative AI, edge intelligence, decentralized machine learning, and incentive mechanism designs.

Yuan Wu (Senior Member, IEEE) received the Ph.D. degree in electronic and computer engineering from The Hong Kong University of Science and Technology in 2010.

He is currently an Associate Professor with the State Key Laboratory of Internet of Things for Smart City, University of Macau, Macau, China, where he is also with the Department of Computer and Information Science. His research interests include resource management for wireless networks, green communications and computing, edge computing and edge intelligence, and energy informatics. He received the Best Paper Award from the IEEE ICC'2016, IEEE TCGCC'2017, IWCMC'2021, and WCNC'2023. He is on the editorial board of IEEE TRANSACTIONS ON VEHICULAR TECHNOLOGY, IEEE TRANSACTIONS ON NETWORK SCIENCE AND ENGINEERING, and IEEE INTERNET OF THINGS JOURNAL.

Xuemin (Sherman) Shen (Fellow, IEEE) received the Ph.D. degree in electrical engineering from Rutgers University, New Brunswick, NJ, USA, in 1990. He is currently a University Professor with the Department of Electrical and Computer Engineering, University of Waterloo, Canada. His research interests include network resource management, wireless network security, the Internet of Things, 5G and beyond, and vehicular ad hoc and sensor networks. He is an Engineering Institute of Canada Fellow, a Canadian Academy of Engineering Fellow, a Royal Society of Canada Fellow, and a Chinese Academy of Engineering Foreign Member. He received the Canadian Award for Telecommunications Research from the Canadian Society of Information Theory (CSIT) in 2021; the R.A. Fessenden Award from IEEE, Canada, in 2019; the Award of Merit from the Federation of Chinese Canadian Professionals (Ontario) in 2019; the James Evans Avant Garde Award from the IEEE Vehicular Technology Society in 2018; the Joseph LoCicero Award and the Education Award from the IEEE Communications Society in 2015 and 2017, respectively; and the Technical Recognition Award from the Wireless Communications Technical Committee in 2019 and AHSN Technical Committee in 2013. He also received the Excellent Graduate Supervision Award from the University of Waterloo in 2006 and the Premier's Research Excellence Award (PREA) from the Province of Ontario, Canada, in 2003. He served as the Technical Program Committee Chair/Co-Chair for IEEE Globecom 2016, IEEE Infocom 2014, IEEE VTC 2010 Fall, and IEEE Globecom 2007, and the Chair for the IEEE Communications Society Technical Committee on Wireless Communications. He is the President of the IEEE Communications Society. He was the Vice President for Technical and Educational Activities, the Vice President for Publications, the Member-at-Large on the Board of Governors, the Chair of the Distinguished Lecturer Selection Committee, and a member of the IEEE Fellow Selection Committee of the ComSoc. He served as the Editor-in-Chief for IEEE INTERNET OF THINGS JOURNAL, *IEEE Network*, and *IET Communications*. He is a registered Professional Engineer of Ontario, Canada, and a Distinguished Lecturer of the IEEE Vehicular Technology Society and Communications Society.

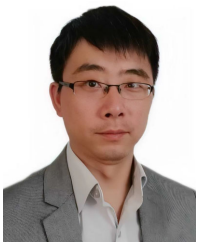

Wenbo Wang (Senior Member, IEEE) received the Ph.D. degree in computing and information sciences from Rochester Institute of Technology, Rochester, NY, USA, in 2016. From 2020 to 2022, he was a Research Fellow with the Faculty of Engineering, Bar-Ilan University, Israel. Before that, he was with the School of Computer Science and Engineering, Nanyang Technological University, Singapore. He is currently an Assistant Professor with the Faculty of Mechanical and Electrical Engineering, Kunming University of Science and Technology, China. His research interests include machine learning and mechanism design for the Industrial Internet of Things (IIoT), prescriptive health management in intelligent manufacturing, and agent AI for unmanned vehicles.